1-1-1979

Astem investigation of grain boundary segregation in impurity doped ceramic oxides.

Barry A. Bender

ASTEM INVESTIGATION OF GRAIN BOUNDARY SEGREGATION IN IMPURITY DOPED CERAMIC OXIDES

by

Barry A. Bender

A Thesis

Presented to the Graduate Committee

of Lehigh University

in Candidacy for the Degree of

Master of Science

in

Metallurgy and Materials Engineering

Lehigh University

1979

CERTIFICATE OF APPROVAL

This thesis is accepted in partial fulfillment of the requirements for the degree of Master of Science.

September 14, 1979
(date)

Professor in Charge

Dr. Alan W. Pense
Chairman, Dept. of Metallurgy & Materials Engineering

ACKNOWLEDGEMENTS

I wish to thank Dr. M. R. Notis, my advisor, for his support and guidance throughout my studies and research. Especially appreciated is his sense of humor that kept things rolling when at times there appeared to be no light at the end of the tunnel. I also wish to thank Dr. D. B. Williams for teaching me how to use the electron microscope and for his input of ideas and suggestions into the project.

The support of the Department of Energy (EY-76-5-02-2408) is also gratefully acknowledged.

I wish to thank the Faculty of the Metallurgy and Materials Engineering Department for the congenial atmosphere they created in and out of the classroom.

I wish to thank Andy Miro for his help in hot pressing the specimens used in this study and for also making our one year spent as roommates interesting. Gratitude is also extended to Al Romig for the microprobe work done in this investigation. Last of all, a special thanks to the members of the Zoo--Steve Baumann, Gay Deamer, Rick Glitz, Spike Narayan, Paul Novotny, Dilip Subramanyam and Carol Weingrod for their humor, craziness, and knowledge that got me through the pitfalls of graduate school.

Finally, I thank my parents, Mr. and Mrs. James A. Bender for their support and encouragement throughout my academic career and my girlfriend Lindsey Vincent for her craziness, companionship, and understanding during these last two years.

TABLE OF CONTENTS

TABLE OF CONTENTS (continued)

LIST OF TABLES

LIST OF FIGURES

LIST OF FIGURES (continued)

ABSTRACT

A scanning transmission electron microscope (STEM) equipped with an energy dispersive spectrometer was used to study solute segregation at the grain boundaries in the systems MgO-NiO, Al_2O_3-Y_2O_3, NiO-Cr_2O_3, and NiO-Al_2O_3. Using the Cliff-Lorimer standardless ratio technique for quantitative X-ray microanalysis and a model which estimated the X-ray volume excited during analysis grain boundary compositions were determined. In Y_2O_3 doped Al_2O_3 grain boundary enrichment of the solute was found to be 240 fold in agreement with auger electron spectroscopy studies of the same system. In NiO doped MgO preferential absorption of the Mg characteristic X-rays by both nickel and oxygen was found to be a critical problem and corrections were required. It was found that this problem is typical of low atomic number oxides. However, preferential absorption of characteristic X-rays by carbon contamination buildup during X-ray analysis was found to be negligible. A grain boundary composition profile was obtained showing no segregation of the nickel to the grain boundary in agreement with current segregation theory. In NiO doped Al_2O_3 and Al_2O_3 doped NiO no solute was detected at the grain boundaries or the matrix. In these cases it appears that either significant absorption effects or impurity concentrations below the minimum mass fraction detectability limit the applicability of analytical STEM (ASTEM). Grain

boundary segregation was measured in the Cr_2O_3 doped NiO. The amount of segregation was determined to be inversely proportional to the solute solubility in accordance with equilibrium segregation theory. As predicted by equilibrium segregation theory the grain boundary composition increased with increasing solute concentration and the amount of grain boundary enrichment decreased with increasing temperature and solute concentration. No difference in microhardness between the grain boundary and the matrix was detected in Cr_2O_3 doped NiO, for which Cr segregation had been directly observed.

I. INTRODUCTION

Solute segregation at grain boundaries can play an important role in the fabrication of ceramics as well as controlling their final physical properties. It has been shown that solute segregation can affect grain growth, electrical and magnetic properties, high temperature creep, fracture strength, toughness, nucleation of phase transformations and sintering properties of ceramic materials.[1,2]

The role of the segregation of densification aids in the sintering of Al_2O_3 has been a point of controversy ever since Jorgensen and Westbrook[3] reported that MgO and NiO segregated in massive amounts to the grain boundaries. Their results were based on autoradiography work, variations of the hardness at the grain boundary, and changes of the lattice parameter with grain size. Tong and Williams[4] using spark source mass spectrometry and Taylor et al.[5] using X-ray photoelectron spectroscopy, also found evidence that MgO solute segregated substantially to the grain boundaries in Al_2O_3. On the other hand, Marcus and Fine,[6] Johnson and Stein,[7] and Nanni et al.[8] using auger electron spectroscopy (AES), found little or no MgO solute segregation to the grain boundaries in Al_2O_3.

These conflicting results may be due to the inherent inadequacies of the above methods used to measure solute segregation. The ideal technique would use an instrument with a resolution of 10 angstroms so that grain boundaries can be directly imaged. This ideal instrument would have the capability to allow one to do

quantitative analysis and to determine the chemical state of the segregating species at the grain boundary itself.[9] A relatively new and powerful analytical instrument that comes close to fulfilling these requirements is the analytical scanning transmission electron microscope (ASTEM). The ASTEM basically consists of an energy dispersive spectrometer (EDS) attached to a scanning transmission electron microscope (STEM). In STEM the electron beam is focused to a fine probe (usually from 10 to 30 nm in diameter) and scanned over the specimen. By positioning this fine probe on the area of interest, X-ray information characteristic of the specimen's composition can be obtained. At the same time crystallographic information can be obtained from microdiffraction techniques and direct high resolution imaging is possible in the conventional TEM mode, all without disturbing the grain boundary structure.

The feasibility of ASTEM to measure solute segregation in metallic systems has already been demonstrated.[10] The purpose of this research was to use ASTEM in the quantitative investigation of solute segregation in various hot pressed impurity doped ceramics. This study discusses the results of the investigation and the method and problems encountered in adapting ASTEM to measure grain boundary segregation in ceramics. Finally, the validity of the indirect technique of using microhardness tests to infer solute segregation will be discussed.

II. BACKGROUND

A. Segregation Phenomena

Segregation phenomena in ceramic materials as compared to metallic systems may occur more frequently and is more complex. The reason is that metals can be purified to less than 1 ppm, while this is difficult to accomplish in most ceramics. Also, due to the high energy for formation of intrinsic defects in ceramics as compared to metals, the role of impurities is critical.[2] As will be discussed later, grain boundary solute segregation has been found to be inversely proportional to the solid solubility limit.[11] Since, in general, ceramic systems have lower solubility limits than metals, segregation should occur more often in ceramics. Further complicating the picture is the electrostatic potential that can build up in ceramics at their grain boundaries due to their ionic nature.[12]

As stated in the introduction, solute segregation can play an important role in controlling the physical properties of materials. However, it was not until McLean[13] came out with his book on grain boundaries in metals in the late 1950's, that a good model of grain boundary solute segregation was developed. Since then extensive research has been conducted on segregation phenomena resulting in several more basic models being developed. The three basic segregation models are the equilibrium segregation model, the non-equilibrium segregation model, and the space charge theory.

(1) Space Charge Theory

Due to the ionic nature of ceramics, electrostatic potentials as great as several tenths of a volt can be built up at the grain boundaries.[2] The space charge is a result of one type of defect being able to form easier than a defect of the opposite sign due to the differences in the free energy of formation of the defects.[14] Since the grain boundaries act as sinks for the excess charged vacancies, a space charge cloud of the opposite charge of 20 to 100 angstroms in width will build up.[1] This space cloud charge can then act as a driving force for solute segregation.

How important of a driving force this phenomena is in ceramics has never been really experimentally shown. The major problem is that to apply the theory, the free energies of formation of vacancies and vacancy-solute binding energies are needed but are unknown for most systems.[1] The work of Yan et al.[15] casts doubt on the importance of the space charge effect and makes the important point that many oxides such as NiO and Al_2O_3 start to lose their ionic nature at higher temperatures and become partial electronic conductors instead.

(2) Non-Equilibrium Segregation

Non-equilibrium segregation is typified by long range solute gradients that can extend up to ten microns away from the grain boundary.[16] These gradients are usually quench rate dependent and can change with time.[17] Non-equilibrium segregation usually manifests itself by increases or decreases in the hardness near the

grain boundaries.[16] It also explains why grain boundary hardness increases with increasing quench rates or quenching from higher temperatures. There are several different theories that model such non-equilibrium segregation phenomena.

A model that often is used is Aust's et al.[18] vacancy-solute theory. In this theory a non-equilibrium concentration of vacancies can be introduced into the system by quenching, sintering, or mechanical deformation. Vacancy gradients develop around sinks such as grain boundaries as the system tries to lower its free energy by the annihilation of excess vacancies at these sinks. Depending on the diffusivities of the solute and the solvent, the solute-vacancy binding energy, and the mobility and the jump frequencies of the solute, solvent, and vacancies a vacancy may drag with it a solute atom.[19] As this pair is driven toward the boundary, it may collide with another pair releasing only one of the vacancies causing a complex to form. This complex may interact with other vacancy-solute pairs to form clusters. The end result being a solute gradient whose concentration increases as one approaches the grain boundary.

(3) Equilibrium Segregation Theory

Equilibrium segregation is typified by solute gradients that extend 10 to 100 nm (one monolayer or at times 2 or 3 layers).[9] Equilibrium segregation does not change with time and the gradient should be reversible upon reheating and recooling. The amount of equilibrium segregation decreases with increasing temperature and

decreasing solute concentration.[13] There have been many models proposed to describe equilibrium segregation. The two that are described here are Hondros'[9] multilayer adsorption theory and McLean's[13] original misfit strain theory.

McLean's model is a statistical thermodynamic approach to the strain energy around solute atoms. The driving force for segregation is the relief of lattice strain by solute atoms segregating to the grain boundaries to fill existing dilated and compressed holes in the interface, thereby reducing strain. In this model several simplifying assumptions are made. One, that the number of atoms at each grain boundary is fixed. Two, that the energy of adsorption onto the lattice is independent of solute concentration. Three, that the entropy change involved in moving solute atoms from the lattice to the grain boundary is the same for all sites and concentrations. Last of all, the vibrational entropy change due to the different masses and interaction potentials of solvent atoms in the grain boundaries are not taken into account.

Using these assumptions and thermodynamics, McLean developed the following expression:

$$C_g = C_m e^{Q/RT}/(1 + C_m e^{Q/RT}) \qquad (1)$$

where C_g is the grain boundary solute concentration, C_m is the bulk solute concentration, and Q is often referred to as the free energy of segregation (ΔG_{seg}) and is equivalent to E-e where E is the distortion energy created by a solute in a lattice site and e is the distortion energy created by a solute in a distorted site found in

the grain boundary. According to this theory, the lower the temperature, the greater the amount of solute segregation. However, the point is made that as one goes to lower temperatures the diffusion kinetics are so slow that massive segregation can not take place.

McLean develops his theory further by saying the free energy of segregation can be related to the strain energy, W, around a solute atom. By elastic theory the strain energy is equal to:

$$W = 24\,K\,G\,r^3\,\epsilon^2/(3K + 4G) \qquad (2)$$

where K is the bulk modulus of the solute, G is the shear modulus of the solvent, r is the radius of the occupied hole, and ϵ, the misfit, equals $(r_1-r_0)/r_0$ where r_1 is the radius of the isolated solute and r_0 is the radius of the unoccupied hole. Johnson[1] says that ΔG_{seg} is proportional to ϵ^2 and that the misfit can be estimated by the difference between the ionic radii of the solvent atom and the solute atom divided by the ionic radii of the solvent atom. One last point is that the saturation of the available sites is approximately equivalent to one monolayer implying that equilibrium segregation is limited to one monolayer.

Hondros and Seah[9] determined experimentally that equilibrium solute segregation could extend to 2 to 3 monolayers. In their work they emphasized the classical thermodynamics approach to segregation showing that the driving force of equilibrium solute segregation is the lowering of the grain boundary energy relative to the bulk, thereby lowering the free energy of the system. In actuality, this theory is the analog of the B.E.T. theory of multilayer gas

adsorption on a surface for a solid/solid interface. At low solute concentration levels, the equation reduces to the following:

$$\frac{X_b}{X_{b_o}} \quad \frac{1}{X_c} = \frac{\exp\ (E/RT)}{X_{c_o}} = B_b \qquad (3)$$

where X_c is the bulk solute concentration, X_{c_o} is the minimum solute concentration needed for precipitation, X_b is the number of moles of solute per unit area of the grain boundary, X_{b_o} is the saturation value of X_b, E is equivalent to $E_1 - E_L$ where E_L is the free energy of solution and E_1 is the free energy of adsorption at the grain boundary and B_b is the grain boundary enrichment ratio. In most of the binary systems that Hondros[11] examined he found that E was in the range of 0-20 KJ/mole implying that:

$$B_b = (1 \text{ to } 10)/X_{c_o} \qquad (4)$$

or that the grain boundary enrichment is inversely proportional to the solid solubility limit as seen in Figure 1. Hondros feels that the solid solubility rule of thumb to predicting solute segregation is a better guide than McLean's ionic radii misfit rule because one really does not know the effective size of a solute atom in a matrix, and since in McLean's model segregation is proportional to the square of the misfit, small errors will be magnified. Also the solid solubility is a better guide to how well a solute atom fits into the matrix as it includes various effects such as valency and atomic misfit.

B. Experimental Technique

The most widely used technique today to directly measure solute segregation at the grain boundaries is AES. The technique has proven quite successful. However, there are still inherent problems with the technique. One is the complexity of AES quantitative analysis. The second is that the grain boundaries are not examined in situ because AES analyses are carried out on grain boundaries exposed by intergranular fracture. As a result only materials that can be fractured intergranularly within the specimen chamber can be examined for solute segregation at the grain boundaries using AES. Another technique that overcomes these two problems is ASTEM. Since the analytical scanning transmission microscope is a relatively new analytical instrument the following section gives a brief description on the operating principles of the instrument.

(1) Analytical Scanning Transmission Microscope

The ASTEM used in this study was a Philips EM300 TEM/STEM equipped with a rear entry NSI EDS detector. The basic operating principle of a TEM/STEM unit is that a fine electron probe is formed and then scanned over the area of interest. By turning off the C_2 lens (condenser lens II) and converting the upper pole piece of the objective lens in a TEM to a strongly convergent lens, the fine probe is formed. Using the scan coils in the dark field controls, the probe can then be scanned across the specimen. Utilizing the imaging system of the TEM the transmitted electrons can

be transferred to an electron detector. The time dependent image is then obtained by applying a scan raster to the detector signal and transferring it to a C.R.T. Once the image is formed the probe can be placed at the point of interest. From the interaction of the beam with the specimen, X-rays characteristic of the composition of the area being probed are collected by the X-ray detector and stored in a multichannel analyzer for analysis. Finally, crystallographic information of the area can be obtained by analysis of convergent beam diffraction patterns whose camera length has been altered through changing the detector collector angle by varying the projector lens current so that all the diffraction spots are visible.

III. EXPERIMENTAL PROCEDURE

A. Materials Analyzed

Hot pressed samples of nominal 10 m/o NiO doped MgO, NiO doped with 0.2 w/o and 1.0 w/o Cr_2O_3, NiO doped with 0.03 w/o and 0.5 w/o Al_2O_3, and Al_2O_3 doped with 0.03 w/o and 0.50 w/o NiO were examined. An experimental sintered alumina fabricated by Coors* doped with 500 ppm Y_2O_3 was also analyzed. The samples were furnace cooled after hot pressing and then examined. The hot pressed Al_2O_3 and MgO samples were fired and then furnace cooled before examination. The Y_2O_3 doped Al_2O_3 was studied in the as-received condition.

B. X-ray Microanalysis

Sections were taken from the hot pressed samples and were mechanically thinned to approximately fifty microns in thickness. Then using a diamond pen, round discs approximately 3 mm in diameter were cut out. These discs were ion thinned using argon at 6KeV at an angle of 15°. The foils were lightly carbon coated and analyzed using the Philips 300 TEM/STEM unit. The foils were placed in a beryllium holder to minimize the interaction with background X-ray counts and tilted to 36° to optimize the count rate.[20] Hole counts were taken to ensure that the level of spurious X-rays was at a minimum[21] (see Figure 2). All specimens were analyzed at 100 KeV using an electron beam of ~ 20 nm in diameter.

---

* Sample courtesy of P. F. Becher, Naval Research Laboratory, Washington, D.C.

To test for solute segregation, point analyses were carried out at both the grain boundary and within the matrix 50 nm away from the grain boundary. All grain boundaries examined were selected so that they were observed to be parallel to the electron beam. The X-ray data were collected for 120 seconds. The X-ray data were then reduced to intensity ratios and compositions were obtained using the Cliff-Lorimer[22] standardless ratio technique for quantitative X-ray microanalysis of thin foils. Grain boundary composition profiles were also determined by placing the electron beam at 50 nm intervals from the grain boundary to examine the extent of solute segregation. Finally, all boundaries probed were examined in TEM for any evidence of grain boundary precipitation.

During the course of this investigation, several problems occurred when trying to use ASTEM to measure solute segregation. As a result several other experiments were undertaken. Two of the experiments dealt with the problem of preferential absorption of elemental characteristic X-rays by the specimen itself and the carbon contamination produced during ASTEM analysis. The third experiment attempted to analyze the actual X-ray volume generated by beam spreading. The results were then compared to an original modification of Doig's and Flewitt's model.[10]

C. Preferential Absorption of Characteristic X-rays by the Matrix

In the initial study of 10 m/o doped MgO, unexpected results were obtained. The data showed that the Ni/Mg X-ray intensity ratios were varying substantially (greater than 10%) from one another. The

problem was assumed to be preferential absorption of the Mg characteristic X-rays by the nickel. To test for absorption effects X-ray intensity ratios were obtained at various thicknesses of the thin foil within one large grain of the material. The thickness of the foil, t, at each position of the probe was measured. This was done as seen in Figure 3 by tilting back to zero degrees and measuring the separation of the carbon contamination spots,[23] d_s, left behind by the probe during analysis. From geometry, the thickness of the foil is:

$$Z = d_s * \cot. 36^{o} \qquad (5)$$

D. Preferential Absorption of Characteristic X-rays by Carbon Contamination

Preferential absorption of the elemental characteristic X-rays of carbon contamination produced during X-ray analysis of thin films of NiAl has been observed by Zalusec and Fraser.[24] The magnitude of preferential absorption by carbon contamination buildup during X-ray analysis was unknown for our instrument. To determine the magnitude of the effect, the variation of the Ni/Mg X-ray intensity ratios (in MgO-10 w/o NiO) with time (increasing carbon buildup) was monitored. This was done by gathering X-ray data from one large grain of homogeneous composition. X-ray intensity ratios were determined at a particular point using 'counting windows' the width of the full peak. This enabled one to obtain the integrated area of the peak minus the background by just switching the 'Net switch' of the multichannel analyzer on and recording the readout. As a result, X-ray

intensity ratios could be determined almost instantaneously allowing the direct comparison of X-ray intensity ratios obtained for different counting times at the same point in the specimen. The various counting times used ranged from 10 to 120 seconds and the resulting intensity ratios were always compared to that X-ray ratio obtained when a count time of 60 seconds was used for the same spot too.

To determine the approximate growth rate of the carbon contamination, STEM micrographs were taken of the spots after 20, 30, 40, 50, 60, and 120 seconds of X-ray analysis at tilts of both 36 and 0 degrees. After inferring from the micrographs that the peaks were conical in shape, the approximate heights and diameters could be derived from the geometry and from the measurements from the micrographs. These dimensions were then plotted against time to determine the empirical growth rate of the spots.

E. X-ray Volume Excited by Beam Spreading

To obtain quantitative results on the amount of solute segregation occurring at grain boundaries, ASTEM analysis requires the approximate X-ray volume excited during analysis. A model was derived estimating this X-ray volume. Therefore, an experiment was needed to test how accurate the model was. The material used was a thin foil of chemically vapor deposited silicon nitride.* A large grain of 10 microns in size was found so that when tilted, well separated thickness fringes were visible. Then using spot sizes (as

---

* Sample supplied from F. S. Galasso of United Technologies Research Center, East Hartford, Connecticut 06108.

listed in the Philips manufacturer's guide to this STEM unit assuming that the fine control of C_1 has been turned all the way clockwise) of 11.5, 20.5 28.5, 39.0, 58.0, and 112.0 nm the net counts of silicon were recorded for at least five different readings at each probe size. The data were then analyzed as presented in the discussion part of the paper.

F. Microhardness Tests

Specimens of hot pressed NiO doped with 1.0 w/o Cr_2O_3 were placed in an alumina crucible and surrounded by powder of the same composition. The specimens were heated to 1548^{o}K for three weeks to allow for grain growth large enough so that microhardness tests would be feasible. The specimens were then furnace cooled, mounted, and polished. After polishing and with the proper lighting the grain boundaries were barely distinguishable. Microhardness measurements using a diamond pyramid indentor and loads of 10 or 50 grams were taken at both the grain boundaries and the matrix. No attempts were made to do a microhardness profile across the grain boundary. Last of all, foils were made from the heat treated specimens and examined with ASTEM for grain boundary solute segregation.

IV. RESULTS AND DISCUSSION

A. Measuring Solute Segregation

Using ASTEM to measure solute segregation quantitatively is not a straightforward procedure. To obtain meaningful results the problems and limitations of the technique must be understood. Sample limitations, instrument related problems, and the limitations of using EDS will be discussed in the following pages. Also the problems involved in quantitative analysis of thin films as well as solute segregation at the grain boundaries will be described in this section.

(1) Sample Limitations

ASTEM analysis is limited to only materials from which thin sections can be produced. Materials with high porosities may not be mechanically strong enough to fabricate a thin section. Ideally, one should strive to produce round thin foils of 3 mm in diameter or otherwise the use of beryllium support grids are needed which further complicates the loading of the specimen into the holder. Also, if the grain size of the material is too large, the electron transparent areas of the foils may not contain a grain boundary to examine.

(2) Instrument Related Problems

From the viewpoint of microanalysis, accelerating voltages of 80 to 100 KeV are needed.[21] With these higher voltages, more counts are generated and the peak to background ratio increases.

However, some materials like the alkali halides may suffer substantial radiation damage at these accelerating voltages and a compromise must be reached. The other problem is the generation of spurious X-rays. The detector should be protected as much as possible from these stray X-rays. To make sure that the spurious X-ray counts are at a minimum, hole counts should be conducted everytime the machine is used.[21] If the counts are too high, unexpected results may occur.

(3) Limitations of EDS

To obtain quantitative information, the net counts of elemental peaks must be determined. Problems arise here with EDS analysis. First of all, EDS can detect only elements from neon and up in the periodic table. Another problem is that the peaks of elements next to one another in the periodic chart may overlap each other. Therefore, ASTEM analysis to measure MgO segregation in alumina would be impractical because the much larger Al peak would cover the minute Mg peak. Next, since the detectability limit of EDS is around 0.5 to 1.0%[25] and the doping levels of the added solute are small, the solute may not be detected at all. Even if peaks are detected they are going to be small. A criterion is needed to tell if the peak is genuine or a statistical variation of the background. Such a criterion has been determined.[26] If the gross count of the peak is $3(2N_B)^{\frac{1}{2}}$ greater than N_B, where N_B is the average background count, then there is only a 0.135% probability that the peak is a statistical fluctuation of the background. One method to improve

the detection of small signals is to increase the number of ev per channel in the counting window as shown by Konig[27] in his theoretical analysis of X-ray intensities as measured by EDS. In this study, instead of using the standard 10 ev per channel, 40 ev per channel were used when attempting to detect small quantities of solute.

(4) Quantitative Analysis of Thin Films

i) Variation of k

Goldstein et al.[28] have shown that the characteristic X-ray intensity of element x, I_x, can be expressed as:

$$I_x = \text{const.}\ C_x\ Q_K\ w_K\ a\ t/A_x \qquad (6)$$

where C_x is the mass concentration of element x, Q_K is the K shell ionization cross section, w_K is the fluorescence yield, t is the thickness of the thin film, A_x is the atomic weight of element x, and a is the ratio of K_α intensity to the total K intensity, $K_\alpha + K_\beta$. Now if the thin film meets the thin film criterion, then X-ray absorption or fluorescence effects can be neglected. From this equation, Cliff and Lorimer developed their standardless ratio technique for quantitative X-ray microanalysis of thin films.[22] Since Q_K, w_K, A_x and a are constant for element x and independent of composition, the X-ray intensity of x is:

$$I_x = C_x\ t/k_x. \qquad (7)$$

Now if the composition of a thin film is known, the thin film acts as its own standard because the measured X-ray intensity ratios for the two elements, x and y, are related to each other by the following equation:

$$I_x/I_y = (C_x/k_x)/(C_y/k_y) \text{ or } C_x/C_y = k_{xy}\ I_x/I_y. \qquad (8)$$

where k_{xy} is the Cliff-Lorimer constant. Since k_{xy} is independent of composition it then can be used to make quantitative measurements on other systems which contain unknown quantities of x and y.

There are several factors that may cause variation in the k ratio. First, k varies with voltage[28] so to obtain accurate results one should always work at the same operating voltage. Experimental work has also shown that k will vary with the technique of determining the X-ray intensity ratio. When quantitative work was being done on MgO doped with 10% NiO the k ratio as determined by computer analysis was different than the value determined 'by hand calculations.' The reason turned out to be that the computer program calculated the X-ray intensities of the peaks in a different manner from the way the net count was being determined 'by hand.' The computer program was counting the area underneath the entire peak and subtracting out the appropriate background counts. The 'by hand' calculations technique was different. Based on experimental results it was found that to obtain X-ray intensity ratios for a system whose concentration was very dilute that a window 200 ev in width be centered around the peak from which a gross X-ray count could be obtained. From this was subtracted the average background count which was obtained from two different windows of 200 ev in width placed on either side of the peak. The end result was that the two different methods yielded different X-ray intensity ratios. As a result one can not interchange X-ray intensity data determined by

the two different techniques in ASTEM quantitative analysis. All X-ray intensities used in this paper were obtained using the 'by hand' technique. It is interesting to note that within the statistical variation expected, that each Ni/Mg X-ray intensity ratio calculated by hand was always 0.9 that of the ratio calculated by the computer program. Last of all, experimentally determined k values for the same element should be expected to vary from instrument to instrument. This is because k will vary with thickness of the Be detector window as well as carbon contamination buildup on such windows.[29] Most likely, different instruments will have different thicknesses for the Be detector window causing k to vary making it impossible to use k values as determined on one instrument in accurate quantitative microanalysis using a different instrument.

ii) Preferential absorption by the matrix

Another important parameter in accurate quantitative X-ray microanalysis is preferential absorption of the elemental characteristic X-rays by the specimen itself. This phenomena has been observed in several metallic systems.[23,30] When analyzing MgO doped with 10% NiO, variation of the X-ray intensity ratios were observed. Preferential absorption by the matrix was pinpointed as the problem. Therefore, the experiment as described earlier was undertaken.

The variation of the Ni to Mg X-ray intensity ratio

as a function of thickness is presented in Figure 4. The data have been reduced so that the plotted points are average characteristic X-ray intensity ratios for a certain range of thickness with the error bars representing the standard deviation from that average value. As shown, the uncorrected ratio increases with increasing foil thickness. Therefore, k_{AB} is thickness dependent, implying that absorption is a problem. Goldstein et al.[28] have given an expression for the correction to the Cliff-Lorimer[22] relationship, to take account of absorption, viz.

$$\frac{C_A}{C_B} = k_{AB} \left(\frac{I_A}{I_B}\right) \exp(-D) \qquad (9)$$

Absorption is considered significant, i.e., the specimen does not satisfy a 'thin film' criterion if $D > 0.1$ where D is given by

$$D = \frac{\rho t}{2} (\chi_B - \chi_A) \qquad (10)$$

where ρ is the specimen density, t the thickness; χ for an element i is given by

$$\chi_i = \left.\frac{\mu}{\rho}\right]^i_{spec} \csc(\alpha) \qquad (11)$$

where $\left.\frac{\mu}{\rho}\right]^i_{spec}$ is the mass absorption coefficient for the characteristic X-ray of element i in the specimen (values are tabulated in the literature[8]) and α is the X-ray take-off angle (36^o).

It was expected that Mg X-rays would be absorbed by the Ni in the specimen, in view of the work of Zaluzec and Fraser,[30] and the uncorrected data in Figure 4 were initially corrected by the

factor exp (-D). The resultant 'partially corrected' data are also shown in Figure 4, and it is clear that there is still significant absorption occurring. However if we take into account the presence of oxygen, although it is not detected by EDS, the total mass absorption coefficient for magnesium in this specimen is:

$$\left[\frac{\mu}{\rho}\right]^{Mg}_{spec} = \left[\frac{\mu}{\rho}\right]^{Mg_K}_{Mg} C_{Mg} + \left[\frac{\mu}{\rho}\right]^{Mg_K}_{Ni} C_{Ni} + \left[\frac{\mu}{\rho}\right]^{Mg_K}_{O} C_O \qquad (12)$$

where C_i is the weight fraction of element i. A similar expression can be written for $\left[\frac{\mu}{\rho}\right]^{Ni}_{spec}$ and these values substituted in Equation (3) to determine the complete correction factor. The fully corrected data are shown in Figure 4, and the slope of the curve has been reduced to zero, which is the desired result for a homogeneous specimen.

Due to the relatively high value of $\left[\frac{\mu}{\rho}\right]^{Mg_K}_{O}$ (2433 cm^2/gm) it can be deduced from Equation (12) that the presence of oxygen will affect all quantitative X-ray microanalysis data in MgO ceramics. It is worth noting here that $\left[\frac{\mu}{\rho}\right]^{Al_K}_{O}$ is 1503 cm^2/gm which indicates that there may be a similar problem in Al_2O_3 although the situation is not so severe.

The uncorrected and corrected data are also shown plotted on log-linear axes in Figure 5. The slope of the fit through the corrected data points is nearly zero showing that the correction factor has solved the problem as the X-ray intensity ratios are virtually independent of thickness. The slope of the best fit through the uncorrected data yields a value for $(\chi_B - \chi_A)$ of

3868 cm^2/gm which compares closely to the theoretical value of 3628 cm^2/gm used to make the corrections, supporting the fact that the variation of intensity with thickness is a result of preferential absorption of characteristic magnesium X-rays by the specimen itself. Also, the y intercept of the line of best fit through the uncorrected data falls almost exactly upon the y intercept of the line of the best fit through the corrected data, again showing the accuracy of the correction factor. From Figure 5 it can be shown that significant (> 5%) absorption will occur at specimen thicknesses > 65 nm, implying that corrections will be needed at all points in a typical thin foil of MgO-10 m/o NiO. Furthermore, even without the presence of nickel, the magnesium X-rays will be absorbed significantly by oxygen at thicknesses $\sim >$ 130 nm. Similar calculations for the effect of oxygen on the Al X-ray intensity show that significant absorption will occur at thicknesses > 160 nm in Al_2O_3. This is also within the range of typical thin foil dimensions.

To emphasize the importance of using absorption corrections in the Cliff-Lorimer ratio technique, the mass fractions of nickel and magnesium were calculated from the corrected and uncorrected ratios. Microprobe analysis on the MgO-10% NiO ceramic confirmed the suspicion that the material was not totally homogenized (bulk composition was 9.2 $\pm$ 1.5%). As a result the material could not be used as its own standard. Therefore, a thin foil consisting of blocks of Mg_2Ni (45.3 w/o Mg and 54.7 w/o Ni) within a ternary mixture of 62 w/o Mg, with 33 w/o Ni and 6 w/o Mo as determined by electron microscope probe analysis was used as the standard.

Absorption corrections were also needed as Mg_2Ni failed the thin film criterion. The resulting k_{NiMg} value was calculated to be 0.82 ± 0.04. Using this value and the uncorrected data, the calculated mole percent of NiO ranged from 10.3 to 13.0 while the corrected data yielded a range of 9.2 ± 0.3 percent. It must be noted again that the difference between the corrected values and the actual composition of 10 mole percent NiO is due to the fact that the sample was determined not to be totally homogenized.

iii) Preferential absorption by carbon contamination

Carbon from contamination buildup absorbs low atomic number elements like magnesium. As a result, Ni/Mg X-ray intensity ratios might be expected to increase with increasing counting times, since the EM300 TEM/STEM is not a high vacuum instrument and contamination in the spot mode of operation can be quite severe.

The results of the variation of the X-ray intensity ratios with counting time are listed in Table I. The experimental deviation, G, is the deviation of the intensity ratios for a particular counting time (I) from the Ni/Mg ratio for 60 seconds of counting (I_{60}) and is given by:

$$G = 100\ (I - I_{60})/I_{60} \qquad (13)$$

The expected statistical deviation, Σ, is calculated using the expression:

$$\Sigma = 100\ [(1 \pm E)*I - I_{60}]/I_{60} \qquad (14)$$

where E is some assumed estimate of the statistical variation in the intensity ratio expected for the low counting rates in ASTEM microanalysis and is given by Cullity[32] as $E = 2.01\sqrt{G/N}$. Here G is the gross number of counts for the characteristic X-ray peak and N is the gross counts minus the background counts. As seen in Figure 6, the experimental deviations for all the various counting times easily lie within the expected statistical deviation range implying that there is no significant variation of the Ni/Mg ratio in the time range of this experiment and therefore with contamination build-up, in this time range.

Theoretical considerations of the problem support this finding. The correction factor to the Cliff-Lorimer relationship for carbon contamination would be

$$C_A/C_B = k_{AB} \ (I_A/I_B) \ e^{-D} \ e^{-F} \qquad (15)$$

where F is given by

$$F = (\mu/\rho]^{B_K}_{carbon} - \mu/\rho]^{A_K}_{carbon}) \ \rho \ x \qquad (16)$$

where ρ is the density of the carbon contamination and x is the path length through the carbon contamination that the characteristic X-rays have to travel through to reach the X-ray detector. In the case of MgO-10 m/o NiO, $\mu/\rho]^{Mg_K}_{carbon}$ is 905 cm^2/gm,[31] and absorption problems might be expected. However, using the thin film criterion, a path length of 555 nm of carbon would be required for F to exceed

0.1, i.e. for absorption to be significant.

To see if this amount of carbon contamination occurs, the growth rate of the spots were determined empirically. From the geometry of the situation as shown in Figure 7, the diameter of the cone of carbon contamination, D, could be estimated by the size of the spot, S, as recorded in a STEM micrograph taken at 36^{o} tilt divided by cos 36^{o}. Determining the peak height of the cone was more involved. Since the actual 3 dimensional picture of the cone was unknown the peak height was considered to be the long side of the cross section of the cone (side c in Figure 7) and a guestimate of the size was the length of the projection of the cone, H, measured from the micrographs taken at 0^{o} tilt divided by the cos 54^{o}. The change in size of the spots with time can be seen in Figures 8 and 9. The average 'peak height' and diameter and standard deviations of the spots for the various times were plotted on linear, semi-log, and log-log axes. The log-log plot as seen in Figure 10 yielded the best fit for the data and implied that the growth rate was a power function. The growth of the diameter of the cone of contamination could be estimated from the slope of line A to be:

$$G_1 = 200\ s^{0.43} \qquad (17)$$

where G_1 is the diameter of the contamination spot in angstroms and s is the counting time in seconds. The estimated growth rate of the 'peak height' taken from curve B of Figure 10 is:

$$G_2 = 540\ s^{0.38}\ . \qquad (18)$$

It was noticed that the ratio of the diameter to the 'peak height'

varied only slightly from 0.45 for all the measurements. Using this knowledge the geometry of the cross section as shown in Figure 7 could be determined. From this, the real peak height (side b) could be estimated and was calculated to be 0.53 G_2. From the same geometry and assuming an average probe diameter (including beam spread) of 50 nm, the longest path of carbon that an X-ray would have to travel through, x, would be:

$$x = (\{0.53\, G_2\}-150)\ \tan 18^{\circ} + 200 \qquad (19)$$

where x is in angstroms.

After 120 seconds the contamination is approximately 160 nm in diameter and 180 nm in height. The longest path length through the contamination is no more than 73 nm. Therefore absorption effects are less than 1.5%, which is less than the expected experimental variation of the X-ray intensity ratios due to low count rates. As a result, if better counting statistics are needed, times of 5 to 10 minutes can be used without any absorption effects (other problems may then become prominent such as specimen drift) from carbon contamination buildup.

(5) Quantitative Analysis of Solute Segregation at the Grain Boundaries

To estimate the grain boundary composition the model of Doig and Flewitt can be used.[10] Their model is shown schematically in Figure 11, where D is the diameter of the electron beam, t is the thickness of the foil at the region being analyzed, and δ is the width of the grain boundary enrichment. Consequently, probe meas-

urements of the grain boundary always will include a substantial contribution (greater than 90%) from the surrounding matrix. From the geometry of the model, the concentration of the solute (cation w/o), C_g, can be related to the concentration of the solute in the matrix, C_M, and the measured concentration at the grain boundary, C_e by the following expression:

$$C_e\ (\pi D^2\ t/4\ ) = C_g\ (D\delta t) + C_M\ (\pi D^2\ t/4 - D\delta t). \qquad (19)$$

This reduces to:

$$C_g = C_M + (C_e - C_M)\ (\pi D/4\ \delta). \qquad (20)$$

Once C_g is known, the grain boundary enrichment ratio can be determined from dividing C_g by C_M, the cation weight percent of the solute in the matrix.

This model has certain limitations. First, δ is an important but unknown parameter. This parameter is hard to measure especially in ceramic systems and it is very sensitive[33] to the thermal history of the sample; reported values vary from 1 to 1500 nm wide. A δ of 1 nm, as observed by various AES studies of grain boundary segregation in metallic systems,[9] was used in all the present calculations.

Another problem is the uncertainty of the diameter of the electron beam, which Doig and Flewitt[10] assumed to be unchanged through the specimen. Due to elastic scatter of electrons, even in thin films, X-rays are generated from a region larger than the diameter of the electron beam. Goldstein et al.[28] have derived an expression for beam spreading:

$$b = 625 \frac{Z}{E_o} (\rho/A)^{\frac{1}{2}} t^{3/2}, \qquad (22)$$

where b is the diameter of the beam in cm, Z is the atomic number, A is the atomic weight, ρ is the density of the film, E_o is the operating voltage in KeV, and t is the thickness of the foil measure in cm. Monte Carlo calculations indicate this equation is a realistic approximation.[25] However, little work has been done in modeling the effective volume of X-ray generation in thin films.

Taking this beam spreading into account a more realistic model to estimate the amount of grain boundary is shown in Figure 13. The model is based upon the assumptions Goldstein et al.[28] used to derive their beam spread expression. Their model (Figure 14) assumes that scattering takes place at the center of the thin film through an angle of ϕ resulting in a beam spread of b. Now if scattering takes place all around the circumference of the electron beam, a truncated cone will be generated. The excited volume can then be represented as shown in Figure 13 as a cylinder (the volume excited by the electron beam without any scattering) whose lower half is surrounded by a truncated cone (the volume excited by elastic scattering). The broadened beam diameter at the bottom of the foil is (D + b). Using geometry the estimate for the solute concentration at the grain boundary is:

$$C_g = C_M + (C_e - C_M) (\pi/6\delta) \left[\frac{6D^2 + b^2 + 3bD}{4D + b} \right] \qquad (23)$$

For the case of no beam spread (b = 0) the equation reduces to the same as Doig's model.

To test how realistic this modification of the Doig-Flewitt model is, the experiment as described previously in the text, was undertaken to estimate the X-ray volume excited. The average number of counts of Si collected for 60 seconds using different probe sizes is listed in Table 2. Since all the measurements in the experiment were taken under identical conditions and since the thickness along a thickness fringe is constant (implying that all measurements were made at the same thickness) the variation in the X-ray counts of silicon collected for different probe sizes should only be related to the X-ray volume excited. If no beam spreading was occurring, then,

$$c_i = k_1 V_i \tag{24}$$

where k_1 is a constant independent of probe size, and c_i is the total number of counts collected in 60 seconds using spot size #i which excites an X-ray volume $V_i (t\pi d_i^2/4)$. Since k_1 should not vary with different probe sizes, then

$$c_i/c_{ii} = d_i^2/d_{ii}^2 \text{ or } c_i/d_i^2 = c_{ii}/d_{ii}^2. \tag{25}$$

As seen in Table 2 this relationship does not hold. This is because beam spreading is occurring and an additional volume of material is excited. As a result, the last expression will not be valid. From the geometry of the schematic of the beam spread model shown in Figure 13, the extra volume excited due to beam spreading, V_{b_i}, is:

$$V_{b_i} = (b^2 + 3\,b\,D)\ (\pi)\ (t)\ /\ 24 \tag{26}$$

and substituting this into equation (24):

$$c_i = k_1 (V_i + V_{b_i}). \qquad (27)$$

Since there are two unknowns in the equation, two sets of data are needed to solve for k_1 and b. In Table 2 there are six sets of data to use to determine b. If the beam spread modification of the Doig-Flewitt model accurately portrays the extra excited X-ray volume, then the b calculated from this experiment should agree with the theoretically calculated b using the Goldstein beam spread formula. Calculations showed that the probe measurements were taken along a contour of the specimen 200 nm in thickness which would lead to an expected beam spread of about 9 nm. The values of b calculated by solving simultaneous equations are listed in Table 3. The data for the large probe sizes (spot sizes 2 and 3) yielded extremely low values. The reason for this might be due to uneven thinning of the specimen. With the much larger beam size the probe will interact with more area and due to uneven thinning the thicknesses of the extra area may be much greater than 200 nm and more volume will be excited and the extra volume will be compensated by lower values of b. The average calculated value of b of 8.7 ± 2.0 nm agrees well with the theoretically calculated value of 9 nm indicating that the model approximates reasonably the extra X-ray volume excited by beam spreading.

The last critical problem in using ASTEM to measure solute segregation is the placement of the electron beam. The model assumes that the beam is centered exactly over the grain boundary. Under typical operating conditions using a 20 nm diameter beam and a δ of

1 nm the grain boundary segregation width is less than 5% of the diameter of the probe as shown in Figure 15. If the beam is placed 8 nm off the center of the grain boundary the effective volume of the grain boundary is reduced by about 50% because, as shown in Figure 15, only half the length of the grain boundary is now being intercepted by the probe. This will reduce the grain boundary enrichment factor by two. This in turn will create greater statistical fluctuations in the X-ray data collected. Working at a magnification of 40,000X, 8 nm is only 0.32 mm which is just greater than the average resolution of the human eye. As a result there will be expected human error in placing the beam. One method that at times overcomes this problem is the centering of the beam on the grain boundary by use of the convergent beam diffraction pattern. This is done by placing the beam so that the intensities of the two diffraction patterns for the two different grains are of equal intensity. However, there is still human judgment involved in determining when the two different diffraction patterns are of equal intensity.

A similar complication is that of specimen drift. Due to the necessity to reduce the statistical uncertainty resulting from low X-ray count rates, counting times of 120 seconds are needed. Since the manufacturer guarantees a drift rate of no greater than 0.1 nm/sec., it is possible that specimen drift may be significant enough so that the beam is not centered over the boundary at all times and additional statistical fluctuations will be expected.

B. Solute Segregation in Various Ceramic Systems

As described in the previous section, ASTEM can be used to quantitatively measure solute concentration at the grain boundaries. ASTEM has certain advantages over techniques such as AES. First of all, most materials can be thinned in some manner so that they can be examined in the electron microscope. Secondly, taking advantage of the excellent resolution in the TEM mode of the TEM/STEM unit, one can directly observe the grain boundary. Last of all, ASTEM quantitative X-ray microanalysis of the grain boundaries is less complex as compared to using Auger electron signals to determine the composition. The major drawbacks of ASTEM are the detectability limits of EDS and the fact that due to beam spreading, the resolution of the technique is much greater than the width of grain boundary enrichment (as predicted by equilibrium segregation) and therefore a value of δ must be assumed. This section discusses the results of using ASTEM to detect segregation phenomena in various ceramic systems in relationship to equilibrium segregation theory. A summary of the experimental results is given in Table 4 and includes appropriate values for k_{AB}, the grain boundary composition C_g, and the enrichment factor (C_g/C_M) for each system studied. Values of C_g and C_g/C_M determined from both the beam-spread and the Doig-Flewitt models are included in this table and it is apparent that there is a major difference between the two models. Clearly beam spreading must always be taken into account in this type of calculation. The more realistic beam spread model always indicates a higher value for both

boundary segregation and enrichment factor.

(1) Solute Segregation in Y_2O_3 Doped Al_2O_3

Johnson et al.[35] and Nanni et al.[8] using AES found that Y_2O_3 segregated to grain boundaries in Al_2O_3. The grain boundary enrichment factor in the two studies varied approximately from 100 to 500 fold. Therefore this system would be a good test of ASTEM capabilities to measure solute segregation. As seen in Figure 17 EDS spectra indicated that no solute was detected in the matrix, but Y was detected at the grain boundary. Using the $3(2\ N_B)^{\frac{1}{2}}$ criterion the recorded peaks were concluded to be the result of segregation. Since the bulk dopant level was below the detectability limit of EDS no X-ray intensity ratios were available from the matrix to calculate k_{YAl}. As a result k_{YAl} was calculated from Equation 6 of Goldstein[28] and estimated to be 2.99 ± 0.58. Nanni et al.[8] determined that the segregation of yttrium was concentrated primarily within a region of 1 nm in width around the grain boundary. Therefore, using a δ of 1 nm in the beam spread model calculations showed that C_g was $12.1 \pm 2.5\%$ or an enrichment factor of 240 ± 50. These results are in good agreement with those obtained with AES indicating that ASTEM can be used to measure solute segregation in a quantitative manner.

(2) Solute Segregation in MgO-10 m/o NiO

Hondros and Seah[9] have shown that, for a number of different metallic systems, the grain boundary enrichment of the solute is inversely proportional to its solid solubility in the matrix. Therefore a system such as NiO in MgO, which shows complete solid solubility,[34] would be expected to show no solute segregation. As

discussed previously since this system shows significant absorption of the Mg characteristic X-rays, by both Ni and oxygen in the specimen, absorption corrections were necessary. The final analysis as seen in Figure 16, which is a typical grain boundary composition profile, indicates that ASTEM can detect no sign of nickel segregation to the boundary. The error bars for all the profiles are the standard deviation from the average calculated composition for that point due to the statistical variation of the experimentally determined X-ray intensity ratios.

(3) Solute Segregation in Cr_2O_3 Doped NiO

In Cr_2O_3 doped NiO, Cr segregation was detected in both the 0.2% and 1.0% Cr_2O_3 doped specimens. EDS evidence for Cr segregation in the 1.0% Cr_2O_3 doped NiO is shown in Figure 18(a) and (b). The collected X-ray data from the Cr peaks in both the matrix and the grain boundary met the $3(2\ N_B)^{\frac{1}{2}}$ criterion. As a result the k_{CrNi} value could be calculated using the X-ray data collected for the chromium peaks in the matrix; the calculated value was $0.70 \pm .10$ as compared with the experimental value of 0.80 ± 0.07 of Cliff and Lorimer.[12] In the 0.2% Cr_2O_3 doped NiO, the Cr peaks collected at the grain boundary (Figure 19(b)) satisfied the $3(2\ N_B)^{\frac{1}{2}}$ criterion but the matrix peaks were borderline (Figure 19(a)). From the grain boundary composition profiles for both doping levels (Figures 12 and 20), it can be inferred that δ, the enriched grain boundary width, is at least less than 50 nm. This is in agreement with the "dedicated STEM" study of Kingery et al.[36] who found impurity segre-

gation in MgO was occurring over a region less than 20 nm.

There is other indirect experimental evidence that supports Cr segregation in NiO. First, in the microhardness experiment etching of the grain boundaries was required. In pure NiO etched 10 seconds in boiling HCl the grain boundaries were clearly attacked. However, after 3 minutes in boiling HCl the Cr_2O_3 doped NiO showed no signs of etching at all. Secondly, Chen[37] and his colleagues in attempting to perform diffusion studies with a Cr_2O_3 doped NiO bicrystal found that additions of Cr_2O_3 to the pure NiO bicrystal made the material extremely brittle. This could be a result of Cr segregation to the grain boundaries. Last of all, the addition of Cr_2O_3 decreased the rate of sintering of NiO substantially. As explained by Jorgensen and Westbrook[3] a solute drag mechanism involving solute segregation to the grain boundaries is one possible explanation for this decrease in the sintering rate.

The calculated values of C_g and the grain boundary enrichment factors (C_g/C_M) are presented in Table 4. These results indicate reasonable agreement with the theories of equilibrium segregation. The NiO-Cr_2O_3 system appears consistent with the behavior noted by Hondros and Seah,[9] that grain boundary enrichment is inversely proportional to the solid solubility. Although there is no phase diagram for the Cr_2O_3-NiO system, some indirectly determined points are available. Meier and Rapp[38] report a solubility limit of 1.1 cation w/o* Cr in NiO at 1373°K and Wood and Hodgkiess[39] report a value between 3.5-4.5% at 1473°K. Using these numbers Cr

*see footnote concerning units in Table 4, p. 53.

segregation in NiO would be expected to be approximately between 20 (i.e., 1/0.045) to 90 (i.e., 1/0.011) fold at the grain boundary which matches well with the experimental measured value at 1443°K (the hot pressing temperature of the 0.2 w/o Cr_2O_3-NiO sample) of 39 ± 6 fold as determined in this study. Also from Greskovich's[40] diffusion study of Cr_2O_3 doped NiO a solubility limit of 7.7 w/o at 1603°K is implied. Interpolating from both Meier's and Rapp's as well as Wood's and Hodgkiess' data, one would expect a solubility limit of Cr_2O_3 in NiO at 1573°K to be between 6.8 and 7.2 w/o. Using these numbers one would expect Cr segregation in NiO at 1573°K to be 16 to 17 fold which matches well with the experimental measured value of 17 ± 4 fold. According to McLean's model,[13] C_g should increase with increasing bulk solute concentration as observed in this study. In addition, equilibrium segregation theory predicts that the enrichment factor should decrease with increasing solute concentration. While this is in fact observed to be true, it is not possible to attribute this with certainty as due to the effect of increasing solute concentration. Since solute segregation also decreases with increasing temperature, and since the 0.2% Cr_2O_3 doped NiO sample was hot pressed at 1443°K while the 1.0% Cr_2O_3 doped sample was hot pressed at 1573°K, the relative extent of the decrease in grain boundary enrichment as controlled by increasing doping level and by increased temperature is unknown.

Another result also indicated that equilibrium segregation was taking place. A specimen of NiO doped with 0.2% Cr_2O_3 was heat

treated at 1473°K for 2 days and then air quenched. Now if equilibrium segregation was occurring the cooling rate should be insignificant and the amount of grain boundary segregation in the quenched sample should be similar to the data for the sample hot pressed at 1443°K and then furnace cooled. ASTEM analysis using the beam spread model showed that C_g was 8.5 ± 3.5% which is close to the value of C_g calculated for 1443°K of 8.3 ± 1.7%. Theoretically, due to the higher temperature C_g for the quenched sample should be lower but due to experimental uncertainty always present in ASTEM as well as imprecise temperature measurements, the data are in good agreement with theory. Based on the three different Cr_2O_3 doped NiO samples and the segregation data obtained using the beam spread model (see Table 4) an estimate of ΔG_{seg} using McLean's isotherm (see equation 1) was calculated to be 43.6 ± 3.6 kJ.

Jorgensen and co-workers[3,41] have inferred the presence of grain boundary segregation by the increase in microhardness detected in the vicinity of grain boundary. This present study has detected no such increase in hardness at the boundary for a system where grain boundary segregation has been directly detected (NiO-Cr_2O_3). The microhardness of the grain boundaries, 547 ± 35 Kg/mm^2, and the matrix, 545 ± 45 Kg/mm^2 of 1.0% NiO doped Cr_2O_3 were the same. While the solutionizing temperatures and final grain size of the annealed specimen are all very different from the hot pressed specimen, ASTEM analysis of the thin foils made from the heat treated specimen (Table 4) still indicated that solute segregation at the

grain boundaries had occurred. Therefore, at least in this system, microhardness data are not a valid test for detecting equilibrium solute segregation at the grain boundaries.

(4) Solute Segregation in the NiO-Al_2O_3 System

The solute species was not detected at either the grain boundaries or in the matrix for 0.03 w/o and 0.5 w/o NiO doped Al_2O_3 or Al_2O_3 doped NiO. One specimen with 0.5 w/o NiO addition, fabricated early in this investigation and apparently not homogenized, contained micron-size inclusions or precipitates of a nickel aluminate spinel. Assuming these particles to be stoichiometric and a typical thin foil thickness of 150 nm the value of k_{AlNi} was found to be 0.81 $\pm$ .05. Cliff and Lorimer[22] determined k_{AlNi} from thin metal foils to be 0.97 $\pm$ 0.11.

The minimum mass fraction (MMF) detectable for an element is given by Goldstein[25] to be:

$$MMF = \frac{3(2I_b^B)^{\frac{1}{2}}}{(I^A - I_b^A)} C_A k_{AB} \qquad (28)$$

where C_A is the concentration and I_A the peak intensity of the solvent species, and the I_b^i terms are the background counts for each of the solvent and solute species. Calculations using experimental X-ray data collected from the nickel aluminate spinel particles give estimated MMF values of $\sim$ 1.8% for Al_2O_3 in NiO, and 0.8% for NiO in Al_2O_3; similar calculations for Cr_2O_3 in NiO indicate an MMF of $\sim$ 0.6%. In addition, significant absorption is expected[20] for Al_2O_3 in NiO, but not for NiO in Al_2O_3 or for Cr_2O_3

in NiO. While equation 28 is only a calculated estimate, the resulting expected MMF for Al_2O_3 in NiO is a factor of three greater than that for Cr_2O_3 in NiO (in fact 0.2 w/o Cr_2O_3 in NiO is barely detectable in the bulk specimen). It is therefore presumed that absorption effects and/or high MMF values result in the lack of detection of Al_2O_3 in NiO and NiO in Al_2O_3 in the matrix at the 0.5 w/o level.

If the calculated MMF values are set equal to the experimentally measured concentrations (C_e) found at the grain boundary, and assuming a typical foil thickness of 135 nanometers, equations 22 and 23 may be used to estimate the grain boundary enrichment necessary before ASTEM analysis would detect it. For 0.5 w/o NiO in Al_2O_3 a grain boundary enrichment of only 3 fold would be required, and for 0.03 w/o NiO this enrichment factor would have to be 320 fold; corresponding enrichments including absorption effects for 0.5 w/o Al_2O_3 and 0.03 w/o Al_2O_3 in NiO would be 130 and 2500 fold respectively. As a result there is no evidence for segregation of Al in NiO. However, even if substantial segregation of Al was taking place it would be undetectable by STEM microanalysis. Similarly there is no evidence for massive segregation of Ni taking place in Al_2O_3 as only 3 fold segregation of Ni to the boundaries would be necessary to detect Ni. Johnson et al.[35] also found no evidence of massive segregation of Ni in Al_2O_3 as their AES studies detected only 2 to 4 fold segregation of Ni to the grain boundaries. They also showed that due to the small ionic radii misfit between

Ni^{++} and Al^{+++} that the observed enrichment of Ni in Al_2O_3 should be only 4 fold.

However, since Johnson et al.[35] found 2 to 4 fold segregation one would expect to detect Ni at the grain boundaries in 0.5% NiO doped Al_2O_3 using ASTEM. Further complicating the issue is that Johnson and Stein[42] found spinel particles in 0.1% NiO doped Al_2O_3 sintered at 2173°K. Since the Al_2O_3 samples in this study were fired at 1673°K the solubility of Ni in Al_2O_3 should be quite low and according to Hondros' model segregation certainly greater than 3 fold should be taking place. The explanation for this discrepancy may be due to a combination of a small grain size and low solute solubility.

From the phase diagram[43] NiO is almost insoluble in Al_2O_3 even at the highest firing temperature of 1673°K used in this study. Peelen[44] has experimentally shown that the solubility of MgO in Al_2O_3 at 1903°K is 300 ppm. Since the unit cells for NiO and MgO are almost identical[45] one might expect the solubility of NiO to parallel that of MgO in Al_2O_3. Johnson and Stein[42] support this saying that their NiO doped Al_2O_3 was an exact analog of their MgO doped Al_2O_3. At a temperature of 1673°K Roy and Coble[39] predict a solubility of 30 ppm MgO in Al_2O_3. Using this number as a ball park figure for NiO solubility in Al_2O_3 the atomic cation fraction of Ni to Al is about 3.5×10^{-5}. Assuming a density of 4 gm/cm^3 and a molecular weight of 100 for Al_2O_3 then the number of Al atoms is:

$$\frac{6 * 10^{23} \text{ atoms}}{\text{mole}} \quad \frac{4 \text{ gm}}{10^{24} \text{Å}^3} \quad \frac{\text{mole } Al_2O_3}{100 \text{ gm}} \quad \frac{2 \text{ moles Al}}{\text{mole } Al_2O_3}$$

$$\simeq 5 * 10^{-2} \text{ Al atoms/Å}^3 \tag{29}$$

Assuming a cubic grain whose edge is 1 micron in length the number of Ni atoms per grain is:

$$\frac{5 * 10^{-2} \text{ atoms Al}}{\text{Å}^3} \quad \frac{[10^4]^3 \text{ Å}^3}{\text{vol. 1 } \mu \text{ grain}} \quad \frac{3.5 * 10^{-5} \text{ Ni atoms}}{\text{Al atoms}}$$

$$\simeq \frac{16.5 * 10^5 \text{ Ni atoms}}{\text{vol. 1 } \mu \text{ grain}} \tag{30}$$

Now the grain boundary volume of the cell can be estimated by assuming a δ of 10 angstroms in width and that each of the 6 faces of the cell are shared by 2 other grains and that all the Ni atoms segregate to the boundary. Then the fraction of Ni atoms per unit volume in the grain boundary is:

$$\frac{16.5 * 10^5 \text{ Ni atoms/1 } \mu \text{ grain}}{(\frac{6}{2})(10\text{Å})(10^4)^2 \text{ Å}^2/1 \mu \text{ grain}} \simeq \frac{5 * 10^{-4} \text{ Ni atom}}{\text{Å}^3} \tag{31}$$

and so C_g is about 1%. Calculations using the MMF equation in conjunction with the beam spread model to determine the solute composition at the grain boundaries indicated segregation of 30% would be needed before segregation could be detected by EDS. As a result the possibility exists that massive segregation is occurring but the enrichment may be substantially limited by the low solid solubility of NiO in Al_2O_3, which limits the number of solute atoms in the matrix that are free to segregate, and by the fact that whatever

atoms are free to segregate must distribute themselves over the relatively larger quantity of grain boundary volume that exists in fine grain size material.

V. SUMMARY AND CONCLUSIONS

A technique has been developed to quantitatively measure equilibrium solute segregation at the grain boundaries using ASTEM. ASTEM offers the advantage that, unlike AES, it is non-selective; meaning that most materials can be studied. The other advantages are that the grain boundary can be directly probed and that quantitative X-ray microanalysis in ASTEM is less complex than most other microanalysis techniques. The major disadvantages are the detectability limits of EDS and a spatial resolution at best of only 20 nm (due to beam spreading) meaning that the area of equilibrium grain boundary enrichment is never directly probed.

Research conducted during the development of the technique revealed that certain parameters must be checked during ASTEM analysis in order to obtain meaningful results:

1. Beam spreading was found to be an important effect and that the extra X-ray volume generated by beam spreading could be reasonably estimated using the beam spread model modification of the Doig-Flewitt model;
2. Preferential absorption of elemental characteristic X-rays by the matrix, especially oxygen in low atomic number oxides like MgO and Al_2O_3, can be significant but the problem can be corrected;
3. Preferential absorption of elemental characteristic X-rays by carbon contamination buildup during X-ray analysis was found to be insignificant;

4. The Cliff-Lorimer k value was found to vary with the technique used to determine the X-ray intensity ratios.
5. For accurate quantitative analysis the level of spurious X-rays must be kept at a minimum, exact centering of the beam over the grain boundary is required, and specimen drift must be kept at a minimum.

ASTEM analysis of various ceramic systems are summarized in Table 4 and below:

1. Grain boundary enrichment levels of 240 fold were detected in Y_2O_3 doped Al_2O_3 which was in good agreement with the AES results reported in the literature;
2. As predicted by Hondros' model relating the amount of grain boundary enrichment to the inverse of the solid solubility of the solute in the matrix, ASTEM analysis of MgO doped with 10 m/o NiO indicates no nickel segregation to the grain boundaries in a system where the solute is completely soluble in the matrix.
3. ASTEM analysis of Al_2O_3 doped NiO detected no signs of Al in the matrix or at the grain boundaries indicating massive segregation was not taking place. However, even if substantial segregation was taking place, due to a high MMF value and strong absorption effects it would be undetected by STEM microanalysis.
4. ASTEM analysis of NiO doped Al_2O_3 detected no signs of Ni in the matrix or at the grain boundaries indicating

massive segregation was not taking place. One explanation for this result is that the ionic radii misfit is not large enough to create the necessary driving force for solute segregation to the grain boundary. However, even though massive segregation is predicted by Hondros' model (due to the low solid solubility of the solute in the matrix) the amount of segregation may be limited by the amount of solute atoms actually free to segregate, which then must distribute itself over the increased grain boundary volume per unit volume found in fine grain size material.

5. Solute segregation was detected in NiO doped with Cr_2O_3 with solute enrichment levels close to those predicted by Hondros' model. Indirect evidence of solute segregation was seen through the differences in the etching, degree of brittleness, and sintering between the pure and doped NiO specimens. The width of the grain boundary enrichment is less than 50 nm. This along with the results of different solute concentrations, temperatures, and cooling rates indicates that equilibrium segregation is taking place. Calculations based on McLean's model indicated that the free energy of segregation is 43.6 ± 3.6 Kj. This value though based on three data points appears to be a reasonable estimate as it falls right in between ΔG_{seg} values calculated for heavy impurity segregation of Y in Al_2O_3 and for inappreciable segregation of Mg in Al_2O_3.[35]

From the results of the various systems it appears Hondros' model for predicting the amount of grain boundary enrichment may be the best. For the system Y_2O_3 doped Al_2O_3, where the valence state is the same for both the solute and the solvent, the space charge model fails to account for the appreciable impurity segregation experimentally observed. However, Y_2O_3 is slightly soluble in Al_2O_3.[34] Using this, the prediction from Hondros' guide agrees well with the amount of segregation reported in this work and by other researchers for this system. For the system Cr_2O_3 doped NiO, where the difference in ionic radii (11%) of Ni^{++} and Cr^{+++} is small, McLean's misfit strain model fails to predict segregation in this system. On the other hand, Hondros' guide predicted quite accurately the amount of grain boundary segregation actually observed in Cr_2O_3 doped NiO. Last of all, Hondros' model predicts the lack of segregation of Ni in NiO doped MgO, which was in agreement with the experimental results.

In the case of NiO doped Al_2O_3 Hondros' model appears not to work. However, due to the low solubility of NiO in Al_2O_3 most of the solute is not going into solution and may be limiting the amount of segregation that can actually take place. This in combination with a grain size effect could inhibit the amount of segregation taking place to the point that the level of segregation is below the detectability limit of ASTEM analysis.

Finally, this study has shown that microhardness may not be a valid technique to infer equilibrium solute segregation at the grain boundaries.

TABLE 1

Ni/Mg X-ray Intensity Ratio for Various Counting Times

Counting Time (seconds)	Ni/Mg X-ray Ratio	Experimental Deviation	Expected Statistical Deviation
10	0.299± 0.030	-3.3%	-16.8% to 10.3%
20	0.307 ± 0.030	0.3%	-4.9% to 5.5%
30	0.318 ± 0.025	3.3%	-0.7% to 7.8%
40	0.314 ± 0.029	1.6%	-1.9% to 5.2%
50	0.311 ± 0.020	0.7%	-2.6% to 3.9%
120	0.309 ± 0.012	0.0%	-2.0% to 2.0%

TABLE 2

Variation of Si Counts with Probe Size

Probe Size Number	Diameter (d_i) of Probe (nm)	Diameter Squared (nm^2)	Total Si Counts Collected	Counts/d_i^2
2	112	12,540	100,385 ± 400	8.00
3	58	3,360	27,212 ± 260	8.09
4	39	1,520	10,210 ± 150	6.71
5	29	810	5,782 ± 60	7.12
6	21	420	3,280 ± 120	7.81
8	12	130	1,179 ± 19	8.92

TABLE 3

Experimentally Determined Values of b

Data Used	b (nm)
Probe sizes 8 and 6	6.8
Probe sizes 8 and 5	8.5
Probe sizes 8 and 4	9.0
Probe sizes 8 and 3	2.3*
Probe sizes 8 and 2	No real solution*
Probe sizes 6 and 5	12.0
Probe sizes 6 and 4	7.4
	$\bar{b} = 8.7 \pm 2.0$

*See page 33 of text for explanation

TABLE 4

Grain Boundary Concentration and Enrichment Factors

Specimen (Dopant)	Segregation	Cliff-Lorimer Ratio (k_{BA})	Grain Boundary Composition (cation w/o) Doig-Flewitt Model	Grain Boundary Composition (cation w/o) Beam-Spread Model	Enrichment Factor (C_g/C_M) Doig-Flewitt Model	Enrichment Factor (C_g/C_M) Beam-Spread Model
Al_2O_3 (0.05 w/o Y_2O_3)	yes	2.99 ± 0.58	9.8 ± 2.0	12.1 ± 2.5	200 ± 40	240 ± 50
MgO (10 mole/o NiO)	no	0.82 ± 0.04	-	-	-	-
NiO (0.2 w/o Cr_2O_3)	yes	0.70 ± 0.10	4.75 ± 1.0	8.3 ± 1.7	22 ± 4	39 ± 6
Air Quenched	yes	0.70 ± 0.10	4.85 ± 1.0	8.5 ± 2.0	23 ± 8	40 ± 14
NiO (1 w/o Cr_2O_3)	yes	0.70 ± 0.10	8.20 ± 1.8	15.3 ± 3.5	9 ± 2	17 ± 4
Annealed	yes	0.70 ± 0.10	5.4 ± 2.4	16.7 ± 8.7	5 ± 2	15 ± 8
Al_2O_3 (0.03 w/o NiO) (0.50 w/o NiO)	not detected	1.23 ± 0.08	-	-	-	-
NiO (0.03 w/o Al_2O_3) (0.50 w/o Al_2O_3)	not detected	0.81 ± 0.05	-	-	-	-

* calculated compositions in the above Table, and as underlined on p. 38 are given as cation w/o; all other compositions are given as either w/o or mole/o as originally specified during alloying of the respective powders.

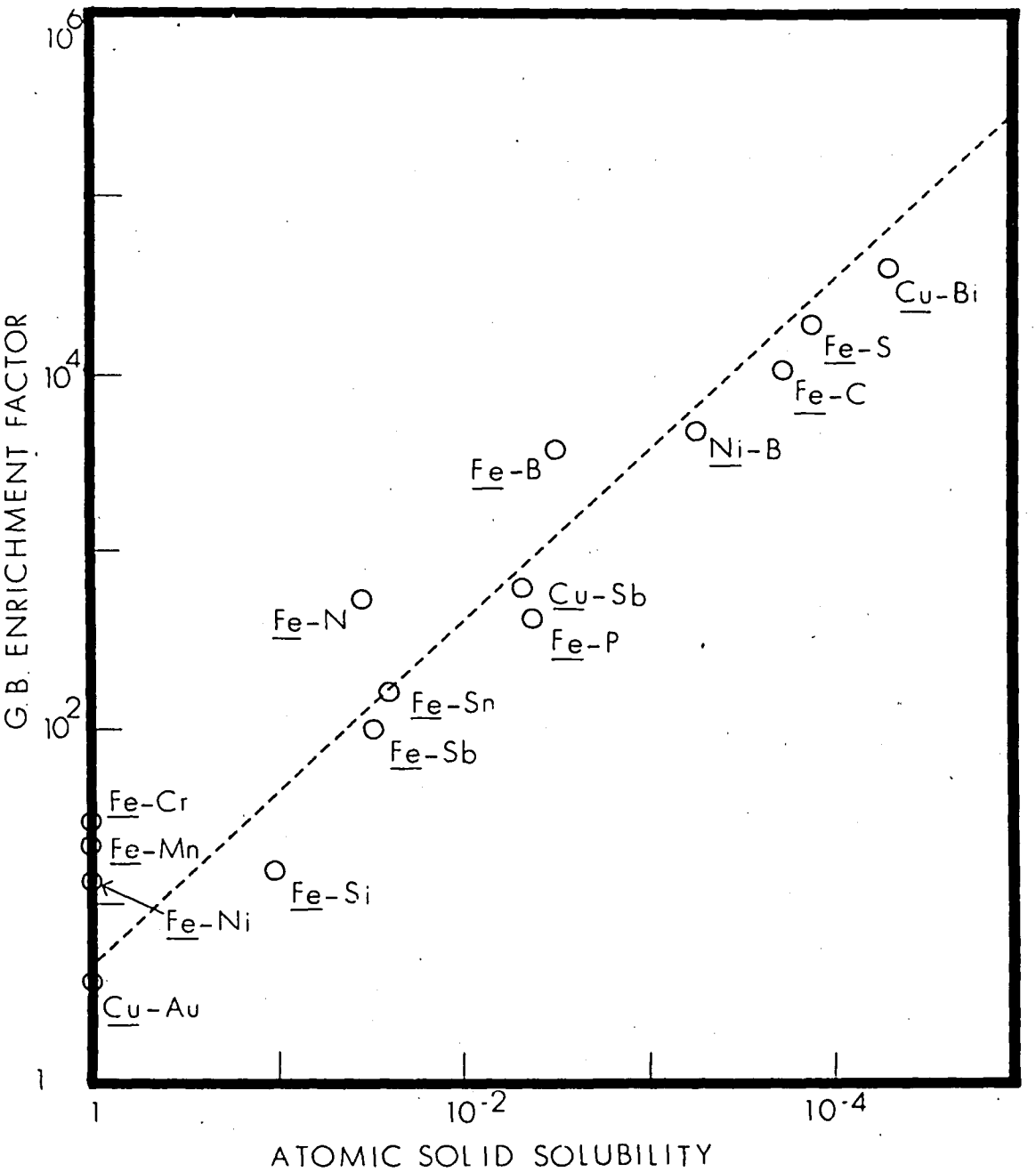

Figure 1. Grain boundary enrichment versus solid solubility. The plot indicates a correlation between grain boundary enrichment and the inverse of solid solubility for a range of systems.[9]

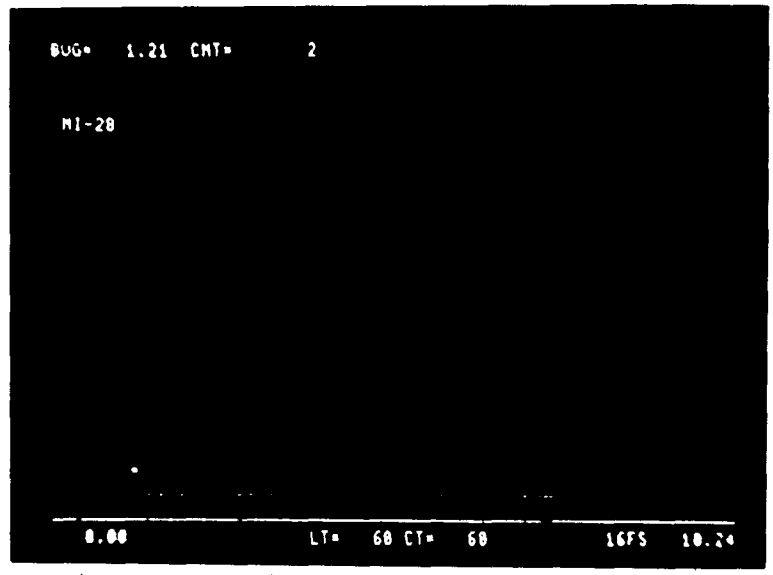

Figure 2. EDS spectrum of a typical hole count. The spectrum shows that the level of spurious X-rays is minimal.

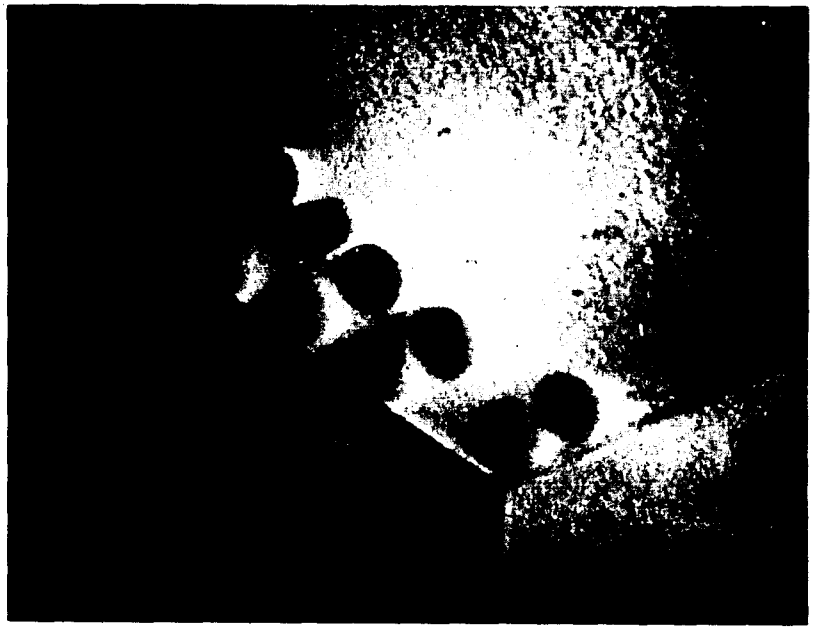

Figure 3. Separation of carbon contamination spots. STEM micrograph showing the projected separation of the contamination spots on the top and bottom of the foil. The micrograph was taken by tilting back to zero degrees after X-ray microanalysis at 36 degrees. Scale bar = 0.5um.

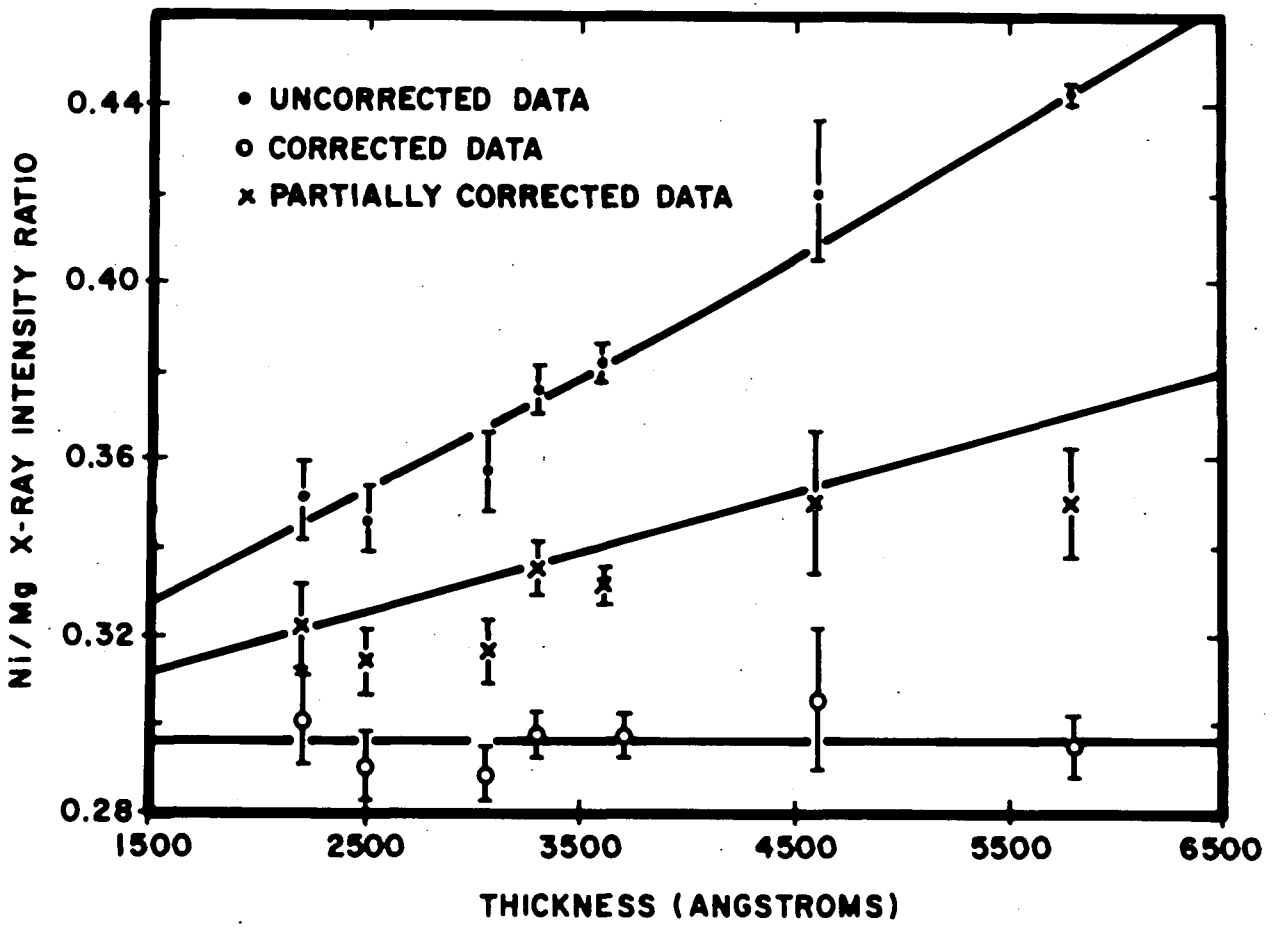

Figure 4. Ni/Mg X-ray intensity ratio as a function of thickness. The uncorrected data indicates the absorption of Mg X-rays is occurring. Partially corrected curve accounts only for absorption by Ni; oxygen absorption effects are included in the fully corrected curve.

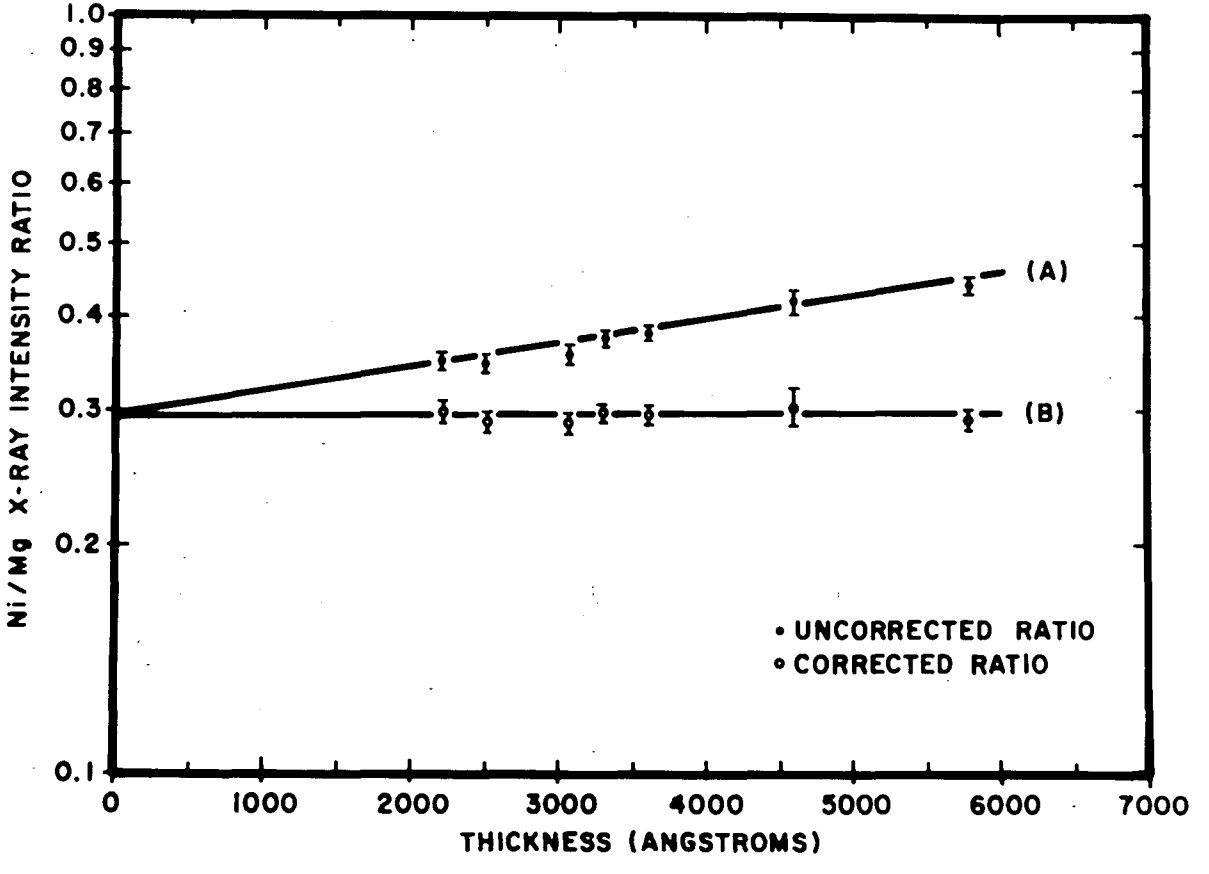

Figure 5. Ni/Mg X-ray intensity ratios as a function of thickness, showing the logarithmic relationship. Extrapolation of both lines to the same point indicates the accuracy of the correction procedure.

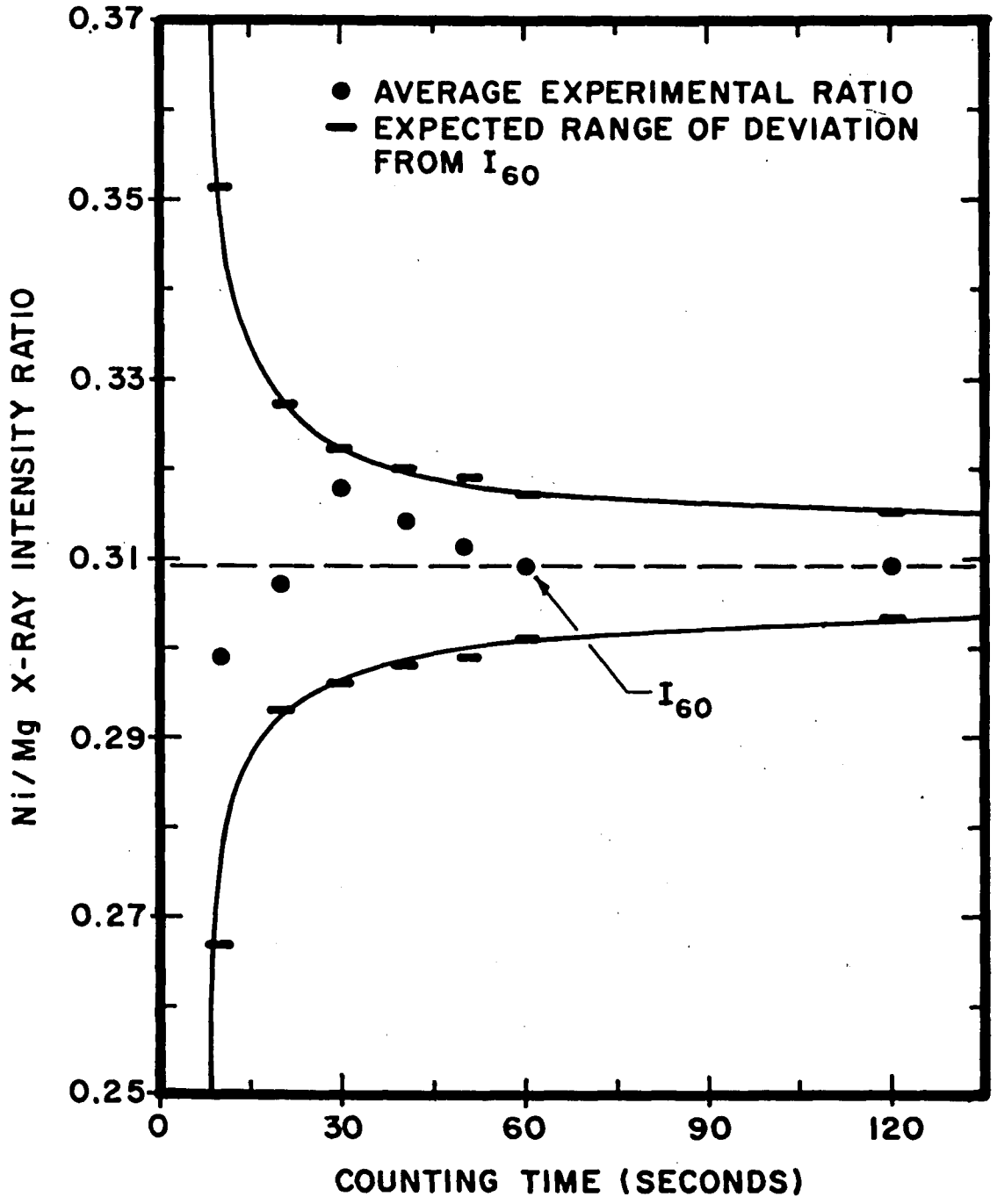

Figure 6. Ni/Mg X-ray intensity ratio versus counting time.

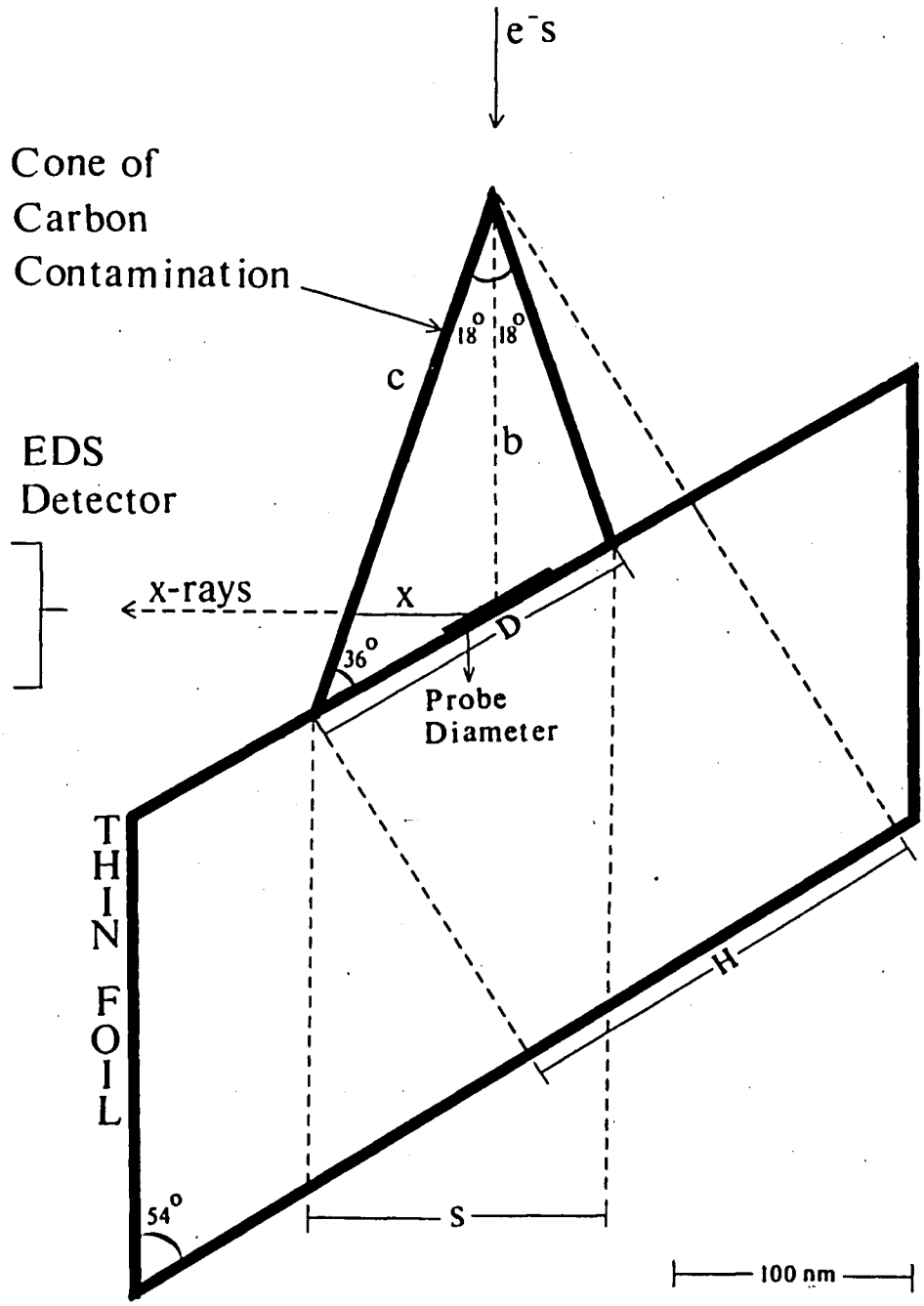

Figure 7. Schematic of a cross section of carbon contamination. The approximate geometry of the vertical cross section is shown of a cone of carbon contamination built up after 120 seconds of X-ray microanalysis.

Figure 8. The growth of carbon contamination after 20 seconds of X-ray microanalysis. Scale bar = 0.5 μm.

Figure 9. The growth of carbon contamination after 50 seconds of X-ray microanalysis. Scale bar = 0.5 μm.

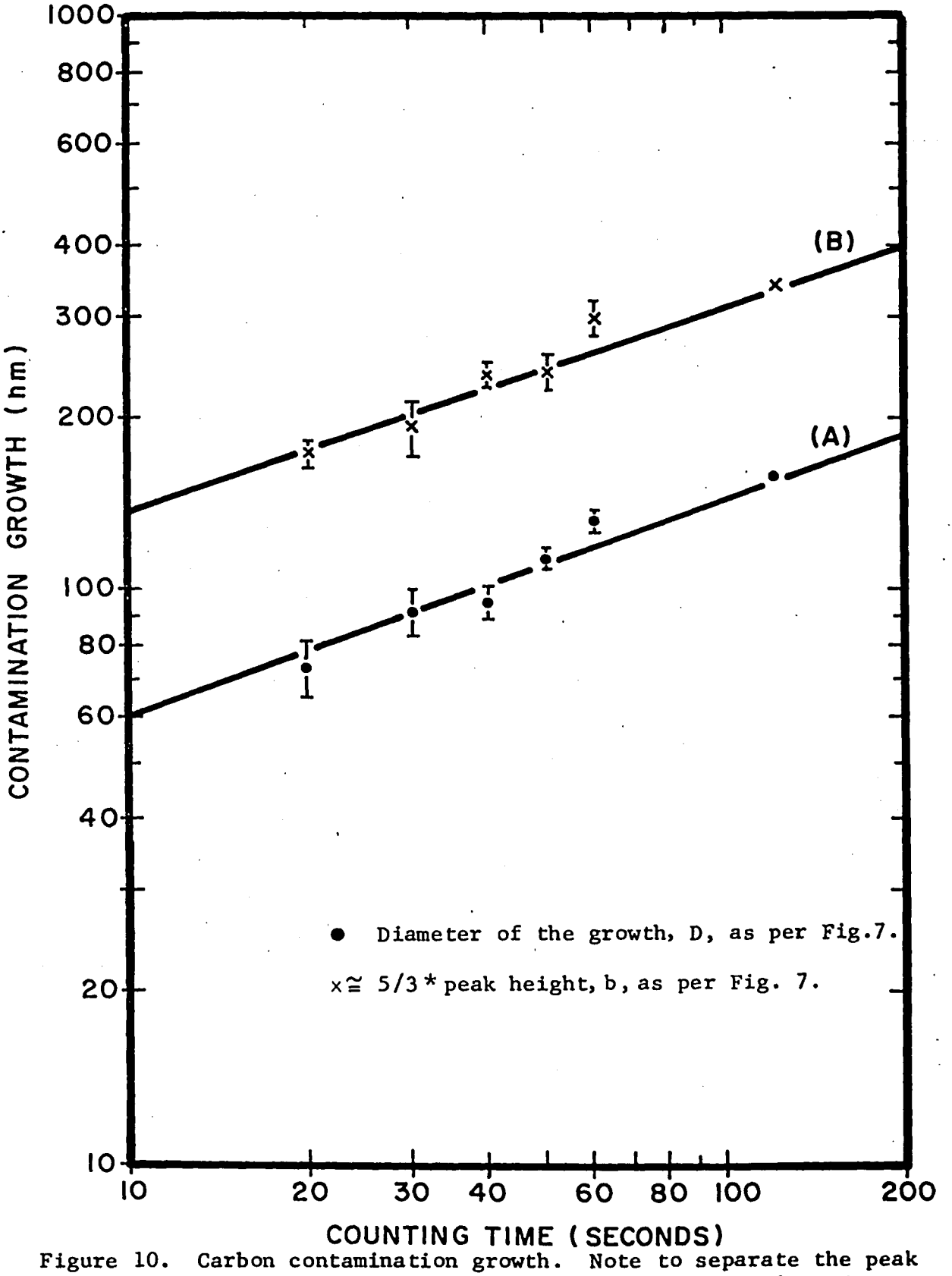

Figure 10. Carbon contamination growth. Note to separate the peak height from the diameter data the peak height data was plotted as 5/3 times the real peak height.

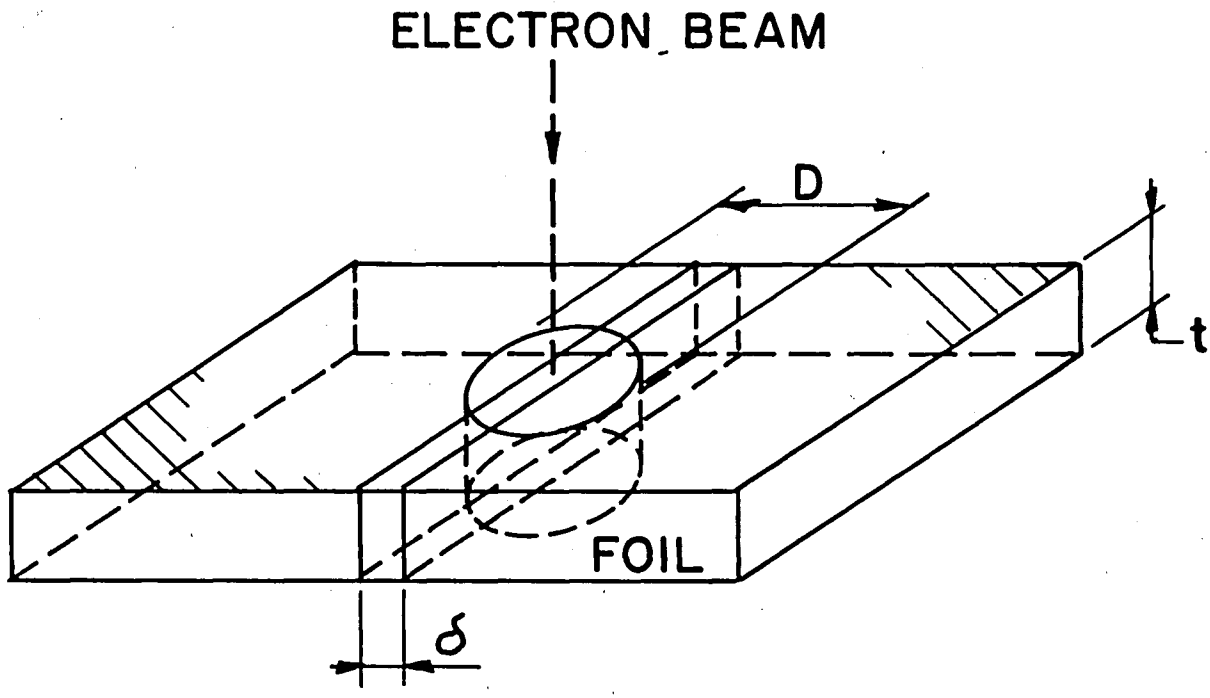

Figure 11. Schematic diagram showing the microanalysis of a grain boundary region using ASTEM.[10]

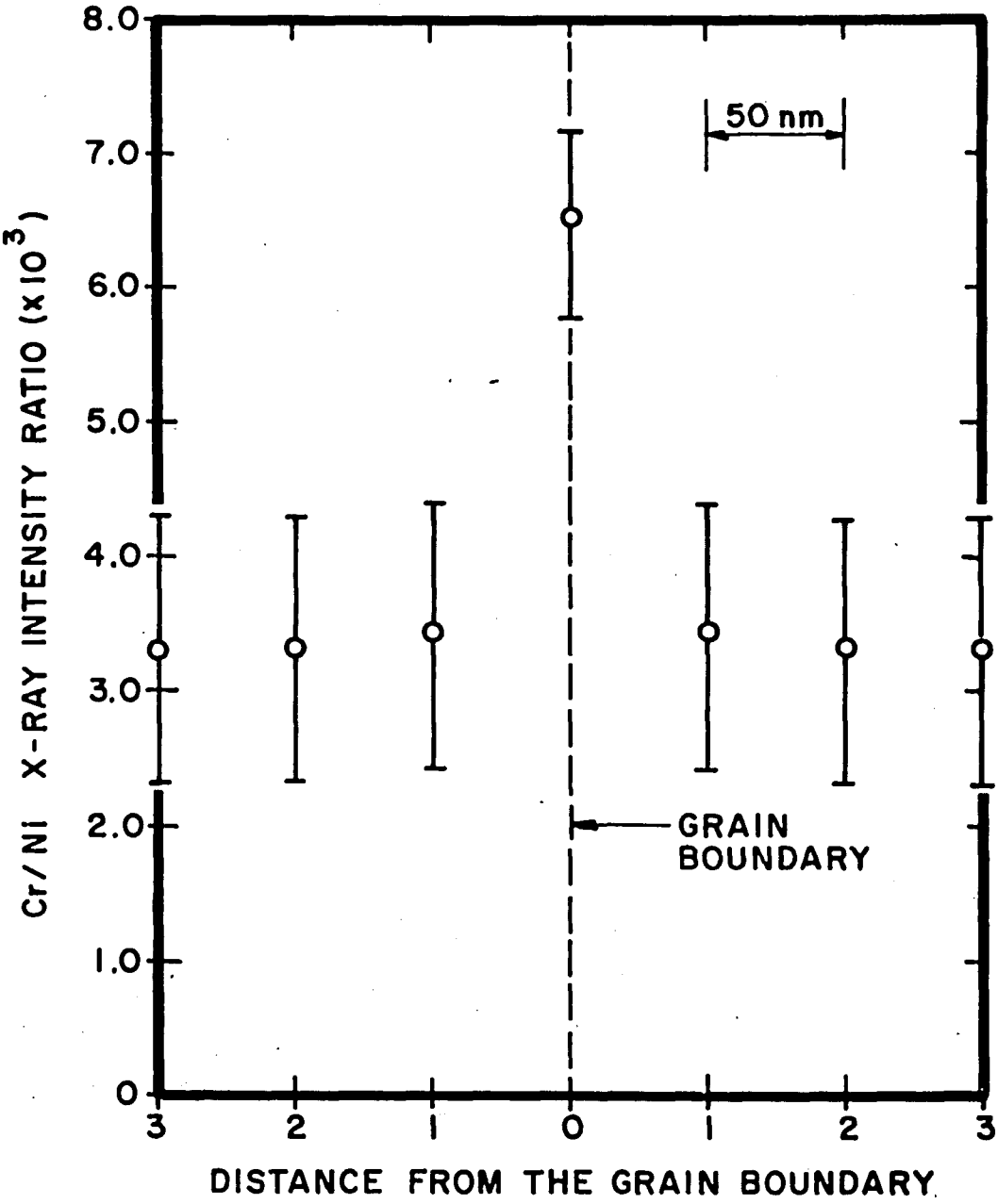

Figure 12. ASTEM grain boundary composition profile of 0.2% Cr_2O_3 doped NiO.

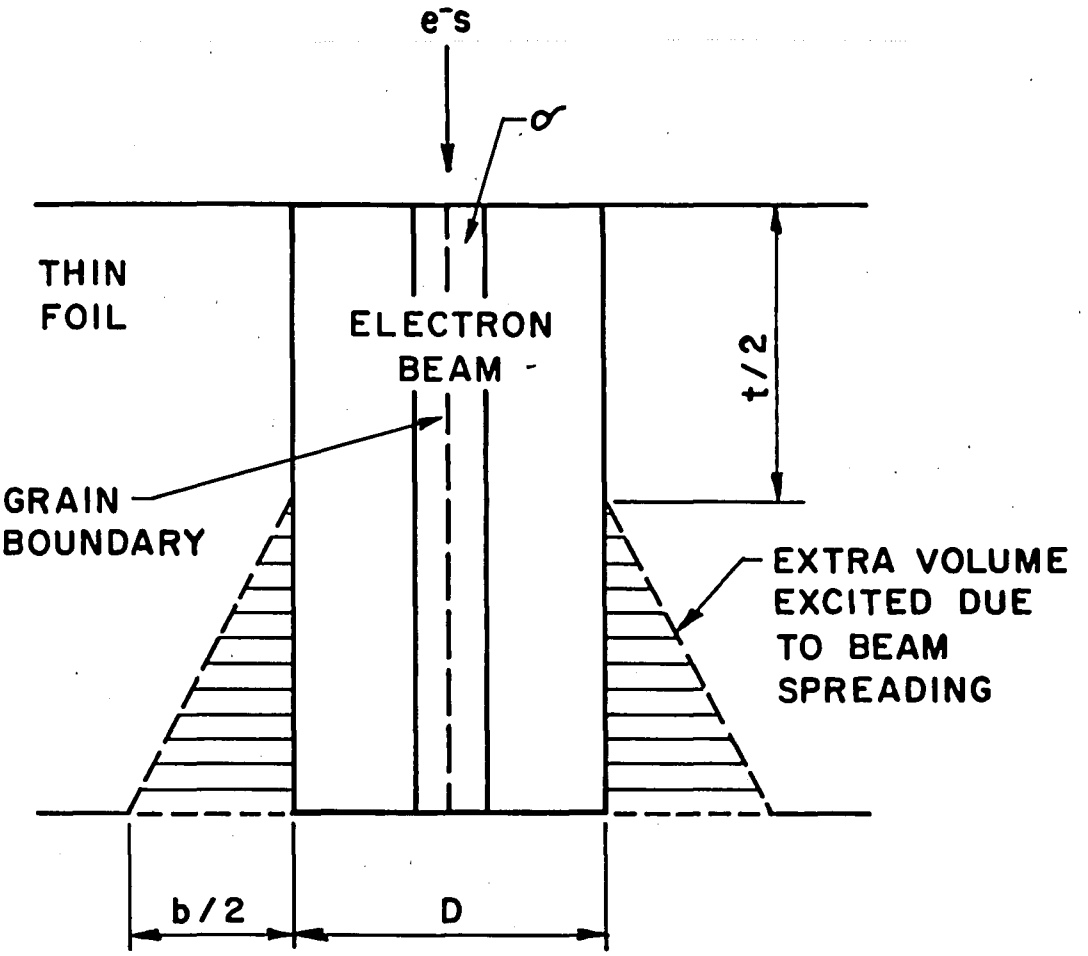

Figure 13. The effect of beam spreading. Schematic diagram shwoing the cross section of the extra X-ray volume excited due to beam spreading from the interaction of the electron beam with the thin foil.

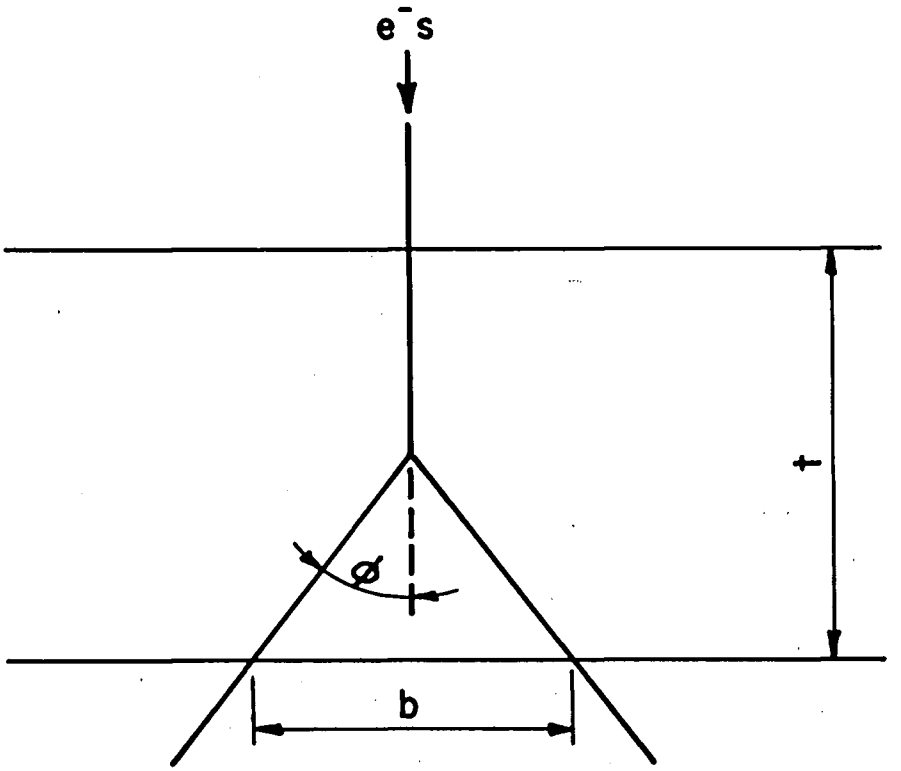

Figure 14. Beam spread model. Goldstein's et al.[28] model for beam spreading (b) in a thin film of thickness t due to single scattering through an angle of ø at the center of the film.

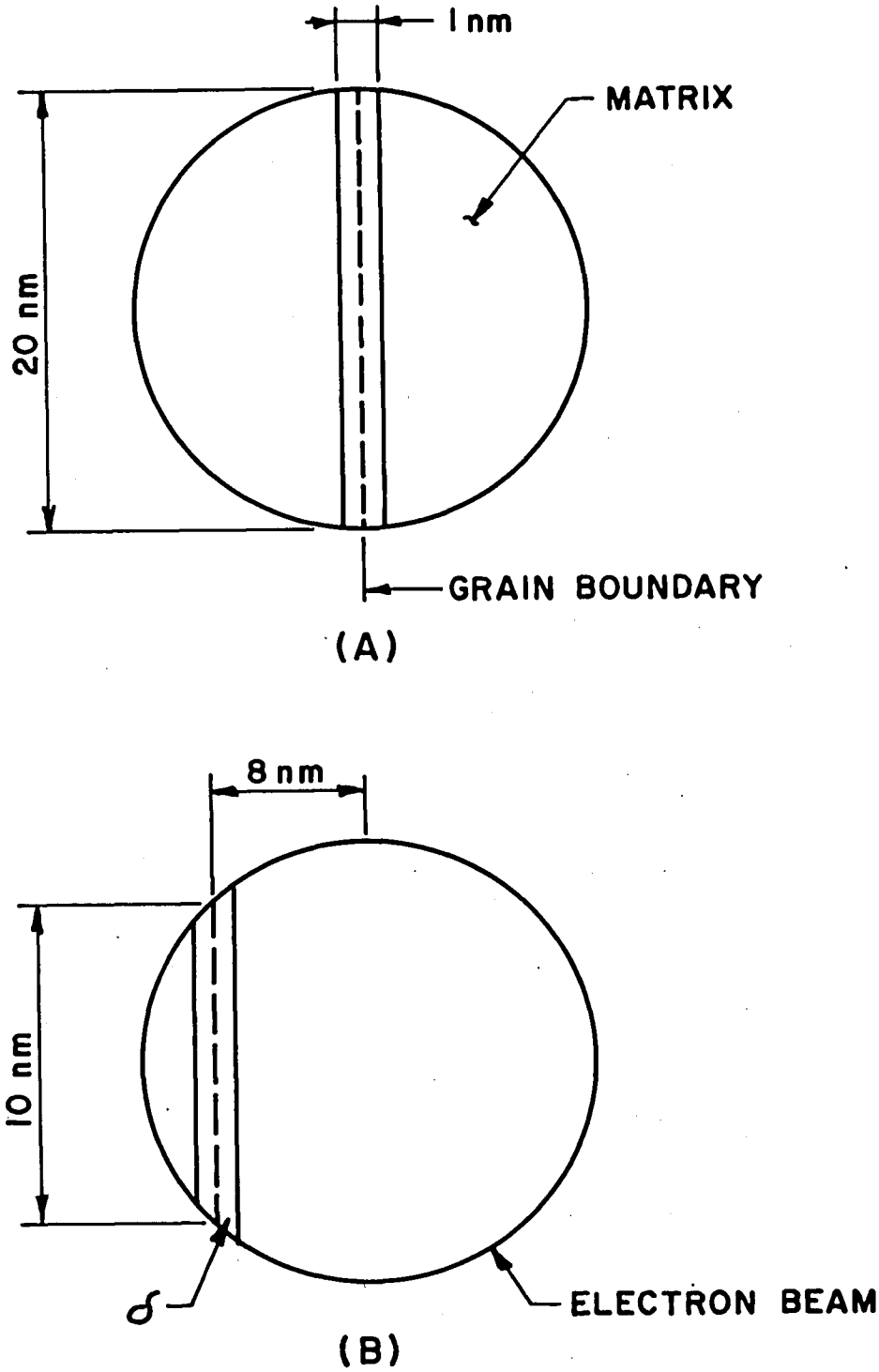

Figure 15. Model emphasizing the importance of the centering of the electron beam over the grain boundary. (A) Accurate placement of the beam; (B) Beam misplaced off-center by only 8 nm resulting in a 50% reduction of the total grain boundary volume being analyzed.

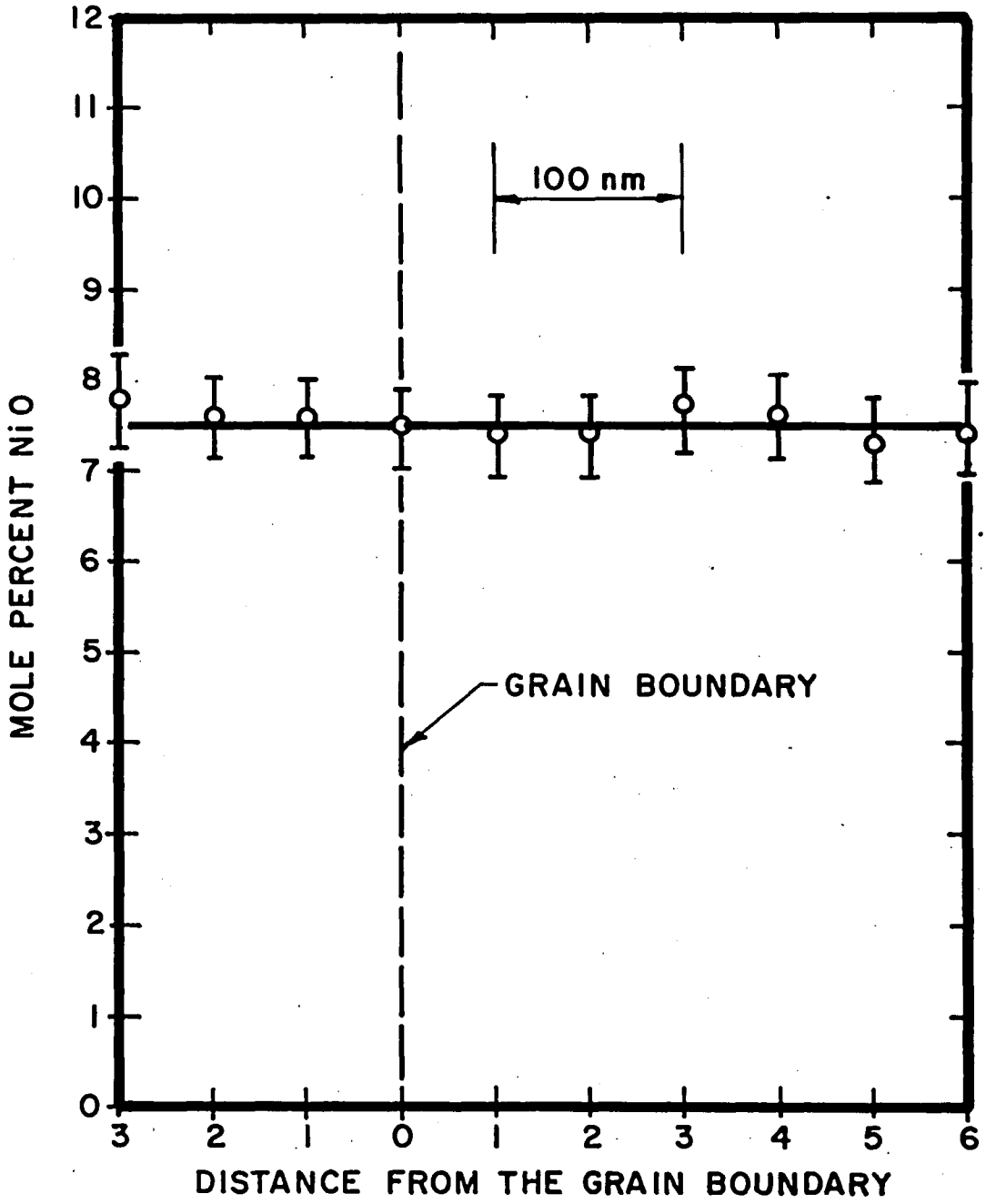

Figure 16. ASTEM grain boundary composition profile of 10 mole percent NiO doped MgO.

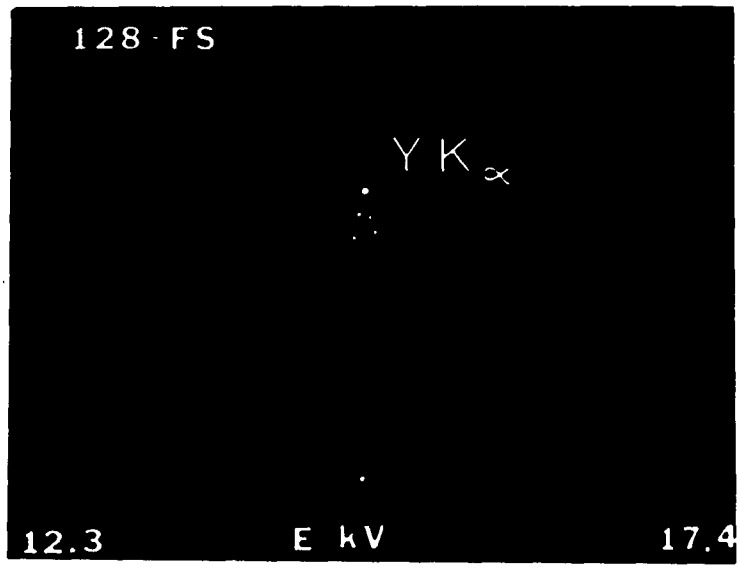

Figure 17. EDS spectra from 500 ppm Y_2O_3 doped Al_2O_3. Upper spectrum: at the grain boundary. Lower spectrum: in the matrix 50 nm from the grain boundary.

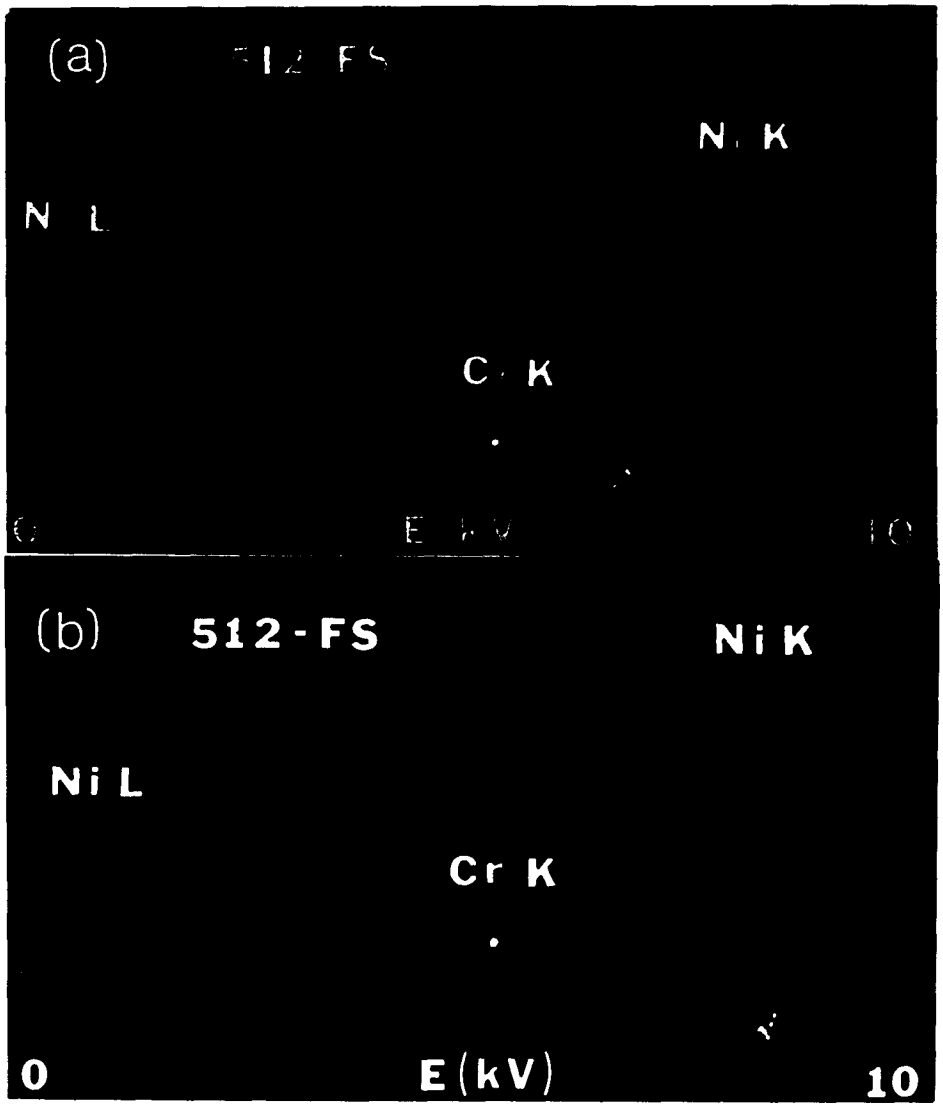

Figure 18. EDS spectra from 1.0% Cr_2O_3 doped NiO. (a) at the matrix 50 nm from the grain boundary; (b) at the grain boundary. Note to make the Cr K alpha peak distinct from the background, the vertical scale has been adjusted resulting in the truncation of the Ni K alpha peak.

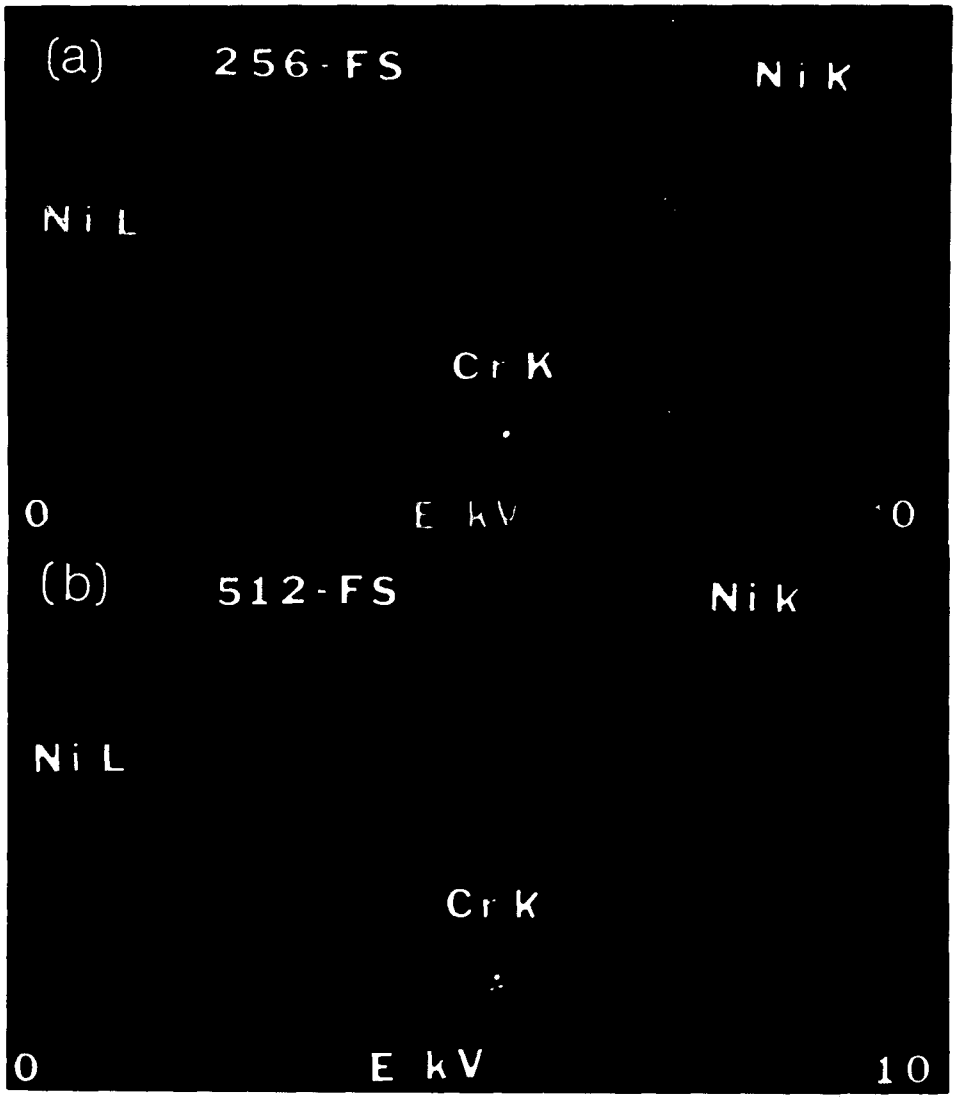

Figure 19. EDS spectra from 0.2% Cr_2O_3 doped NiO. (a) at the matrix 50 nm from the grain boundary; (b) at the grain boundary. Note to make the Cr K alpha peak distinct from the background, the vertical scale has been adjusted resulting in the truncation of the Ni K alpha peak.

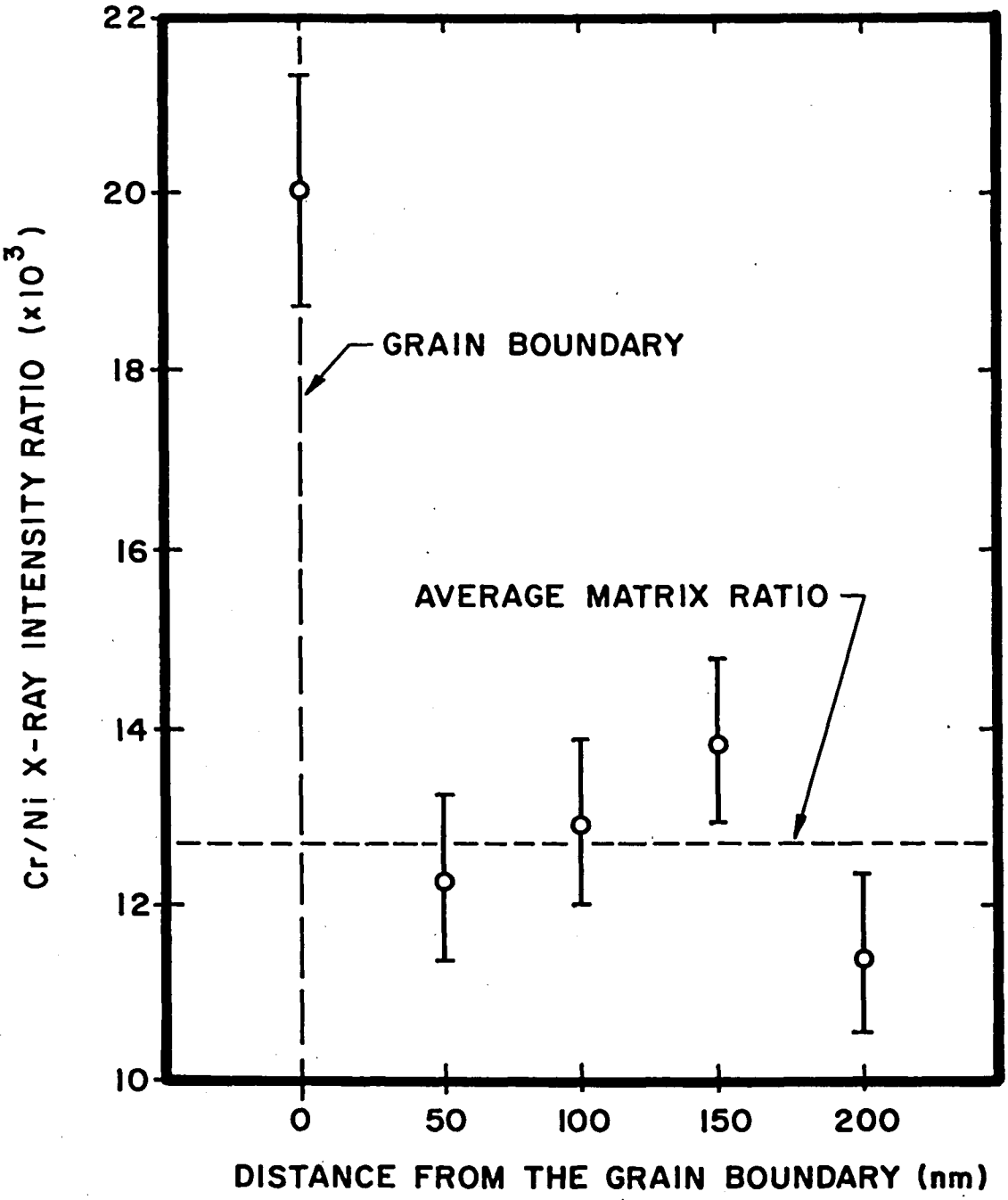

Figure 20. ASTEM grain boundary composition profile of 1.0% Cr_2O_3 doped NiO.

REFERENCES

1. W. C. Johnson, "Grain Boundary Segregation in Ceramics," Met. Trans. A, 8A 1413-1421 (1977).
2. W. D. Kingery, "Plausible Concepts Necessary and Sufficient for Interpretation of Ceramic Grain-Boundary Phenomena: I. Grain Boundary Characteristics, Structure and Electrostatic Potential" J. Am. Ceram. Soc., 57(1) 1-8 (1974).
3. P. J. Jorgensen and J. H. Westbrook, "Role of Solute Segregation at Grain Boundaries During Final-Stage Sintering of Alumina," J. Am. Ceram. Soc., 47(7) 332-338 (1964).
4. S. S. C. Tong and J. P. Williams, "Chemical Analysis of Grain Boundary Impurities in Polycrystalline Ceramic Materials by Spark Source Mass Spectrometry," J. Am. Ceram. Soc., 53(1) 58-59 (1970).
5. R. I. Taylor, J. P. Coad and R. J. Brook, "Grain Boundary Segregation in Al_2O_3," J. Am. Ceram. Soc., 55(11) 568-570 (1972).
6. H. L. Marcus and M. E. Fine, "Grain-Boundary Segregation in MgO-Doped Al_2O_3," J. Am. Ceram. Soc., 55(11) 568-570 (1972).
7. W. C. Johnson and D. F. Stein, "Additive and Impurity Distributions at Grain Boundaries in Sintered Alumina," J. Am. Ceram. Soc., 58(1-2) 485-488 (1975).
8. P. Nanni, C. T. H. Stoddart and E. D. Hondros, "Grain Boundary Segregation and Sintering in Alumina," Mat. Chem. 1, 297-320 (1976).

9. E. D. Hondros and M. P. Seah, "Segregation to Interfaces," Int. Rev., Review #222, 262-301 (1977).

10. P. Doig, R. K. Wild and P. E. J. Flewitt, "A Comparison of X-ray (STEM) and Auger Electron Spectroscopy for the Micro-analysis of Grain Boundary Segregation," Berkeley Nuclear Laboratory, England, prepared for the Central Electricity Generating Board, SS D/SE/r14/78 (Jan. 1978).

11. E. D. Hondros, "Grain Boundary Segregation the Current Situation and Future Requirements," J. Phys. 36(C4) 117-134 (1975).

12. K. Lehovec, "Space-Charge Layer and Distribution of Lattice Defects at the Surface of Ionic Crystals," J. Chem. Phys., 21(7) 1123-1128 (1953).

13. D. McLean, Grain Boundaries in Metals, pp. 116-149, Clarendon Press, Oxford, 1957.

14. K. L. Kliewer and J. S. Koehler, "Space Charge in Ionic Crystals. I. General Approach with Application to NaCl," Phys. Rev., 140(4A) 1226-1240 (1965).

15. M. F. Yan, R. M. Cannon, H. K. Bowen and R. L. Coble, "Space Charge Contribution to Grain-Boundary Diffusion," J. Am. Ceram. Soc., 60(3) 121-127 (1977).

16. J. H. Westbrook, "Impurity Effects at Grain Boundaries in Ceramics," Science of Ceramics, Vol. 3, pp. 263-284, Academic Press, New York, 1967.

17. H. Gleiter and B. Chalmers, "High-Angle Grain Boundaries," Progress in Materials Science, Vol. 16, pp. 1-65, Pergamon

Press, New York, 1972.

18. K. T. Aust, R. E. Hanneman, P. Niessen and J. H. Westbrook, "Solute Induced Hardening Near Grain Boundaries in Zone Refined Metals," Acta. Met. 16(3) 291-303 (1968).

19. R. E. Hanneman and T. R. Anthony, "Effects of Non-Equilibrium Segregation on Near-Surface Diffusion," Acta. Met., 17(9) 1133-1140 (1969).

20. R. H. Geiss and T. C. Huang, "Quantitative X-ray Energy Dispersive Analysis in the Transmission Electron Microscope," X-ray Spectrometry, 4, pp. 196-201 (1975).

21. J. I. Goldstein and D. B. Williams, "X-ray Analysis in the TEM/STEM," Scanning Electron Microscopy/1977, Vol. 1, pp. 651-662, IIT Research Institute, Chicago, 1977.

22. G. Cliff and G. W. Lorimer, "Quantitative Analysis of Thin Metal Foils Using EMMA-4, The Ratio Technique," Proc. Fifth Europ. Cong. on EM, pp. 203-207, Institute of Physics, London, 1972.

23. G. W. Lorimer, G. Cliff and J. N. Clark, "Determination of the Thickness and Spatial Resolution for the Quantitative Analysis of Thin Foils," Developments in Electron Microscopy and Analysis, EMAG 75, pp. 153-156, Academic Press Inc., London, 1976.

24. N. J. Zaluzec and H. L. Fraser, "On the Effects of Contamination in X-ray Microanalysis," Analytical Electron Microscopy, Report of a Specialist Workshop, pp. 122-129, Cornell Univ., Ithaca, NY 1978.

25. J. I. Goldstein, "Principles of Thin Film X-ray Microanalysis," in Principles of Analytical Electron Microscopy, Plenum Press, New York, 1979.

26. J. I. Goldstein and J. W. Colby, "Special Techniques in the X-ray Analysis of Samples," Practical Scanning Electron Microscopy, pp. 451-456, Plenum Press, New York, 1975.

27. R. Konig, "Quantitative X-ray Microanalysis of Thin Foils," Electron Microscopy in Mineralogy, pp. 526-536, Springer-Verlag, New York, 1976.

28. J. Goldstein, J. Costley, G. Lorimer and S. Reed, "Quantitative X-ray Analysis in the Electron Microscope," Scanning Electron Microscopy/1977 Vol. 1, pp. 315-324, IIT Research Institute, Chicago, 1977.

29. S. Mehta, J. I. Goldstein, D. B. Williams and A. D. Romig, "Determination of Cliff-Lorimer k Calibration Factors for Thin Foil X-ray Microanalysis of Na, Mg and Al in the STEM," paper to be published.

30. N. J. Zaluzec and H. L. Fraser, "Microchemical Analysis of Thin Metal Foils," Proc. 34th Annual EMSA Meeting, pp. 420-421, Claitor's Publ. Div., Baton Rouge, 1976.

31. T. D.McKinley, K. F. J. Heinrich and D. B. Wittry, eds., The Electron Microprobe, pp. 351-352, Wiley, New York, 1966.

32. B. D. Cullity, Elements of X-ray Diffraction, pp. 204-205, Addison-Wesley, Mass., 1956.

33. P. J. Jorgensen, "Grain Boundary Phenomena in Ceramic Materials," Proceedings of the Fourth Bolton Landing Conference, pp. 205-221, Claitor's Pub. Div., Baton Rouge, 1975.

34. E. M. Levin, C. D. Robbins and H. R. McMundie, Phase Diagrams for Ceramists, p. 110 and 122, American Ceramic Society, Inc., Columbus, 1964.

35. W. C. Johnson, D. F. Stein and R. W. Rice, "Grain Boundary Chemistry in Sintered Al_2O_3 and Hot Pressed MgO," Proceedings of the Fourth Bolton Landing Conference, 261-274, Claitor's Pub. Div., Baton Rouge, 1975.

36. W. D. Kingery, T. Mitamura, J. B. Vander Sande and E. L. Hall, "Boundary Segregation of Ca, Fe, La and Si in Magnesium Oxide," J. Mat. Sci., 14(7) 1766-1767 (1979).

37. Private communication with Dr. W. K. Chen of Argonne National Laboratories, Argonne, Ill. 60439.

38. G. H. Meier and R. A. Rapp, "Electrical Conductivities and Defect Structures of Pure NiO and Chromium-Doped NiO," Zeit. phys. Chemie, N.F. 74 168-189 (1971).

39. G. C. Wood and T. Hodgkiess, Nature (London), 211 1358 (1966).

40. C. Greskovich, "Kinetics of $NiCr_2O_4$ Formation and Diffusion of Cr^{3+} Ions in NiO," J. Am. Ceram. Soc., 53(9) 498-502 (1970).

41. P. J. Jorgensen and R. C. Anderson, "Grain-Boundary Segregation and Final-Stage Sintering of Y_2O_3," J. Am. Ceram. Soc. 50(11) 553-558 (1967).

42. W. C. Johnson and D. F. Stein, "Additive and Impurity Distributions at Grain Boundaries in Sintered Alumina," J. Am. Ceram. Soc., 58 (11-12) 485-488 (1975).

43. B. Philips, J. J. Hutta and I. Warshaw, "Phase Equilibria in the System NiO-Al_2O_3-SiO_2," J. Am. Ceram. Soc., 46 (12) 579-583 (1963).

44. J. G. J. Peelen, "Influence of MgO on the Evolution of the Microstructure of Alumina," Materials Science Research, Vol. 10, pp. 443-453, Plenum Press, N.Y. 1975.

45. ASTM X-ray File Cards #4-0829 and 4-0835.

46. S. K. Roy and R. L. Coble, "Solubilities of Magnesia, Titania and Magnesium Titanate in Al_2O_3," J. Am. Ceram. Soc., 51(1) 1-6 (1968).

VITA

Barry A. Bender was born to Mr. and Mrs. James A. Bender on September 2, 1954 in Platte, South Dakota. He went to highschool at James Madison Highschool, Vienna, Virginia. In September of 1972 he entered Virginia Polytechnical Institute and State University at Blacksburg, Virginia. At the end of his freshmen year he entered the Cooperative Education Program working in the ceramics branch at the Naval Research Laboratory in Washington, D. C. In his junior year he played varsity soccer and lettered in his senior year. He graduated in May of 1977 with a Bachelor of Science Degree in Metallurgical Engineering.

In August of 1977, he entered Lehigh University in the Department of Metallurgy and Materials Engineering. While in graduate school he was elected to the national scientific honorary society of Sigma Xi. He has participated in intramural soccer, softball, volleyball, and the Turkey Trot. He is a member of ASM-AIME, ACS, NICE, and the national honorary societies of Alpha Sigma Nu, Tau Beta Pi, and Phi Kappa Phi.